




Article

Performance of Self-Compacted Geopolymer Concrete Containing Fly Ash and Slag as Binders

Aryan Far H. Sherwani ^{1,2,*} , Khaleel H. Younis ^{3,4} , Ralf W. Arndt ^{2,*} and Kypros Pilakoutas ⁵ 

¹ Department of Civil Engineering, Faculty of Engineering, Soran University, Soran 44008, Kurdistan Region, Iraq

² Department of Civil Engineering, Fachhochschule Erfurt-University of Applied Sciences, 99084 Erfurt, Germany

³ Department of Surveying and Road Construction, Erbil Technology College, Erbil Polytechnic University, Erbil 44001, Kurdistan Region, Iraq

⁴ Civil Engineering Department, Tishk International University, Erbil 44001, Kurdistan Region, Iraq

⁵ Civil and Structural Engineering Department, University of Sheffield, Sheffield S13JD, UK

* Correspondence: arianfar.abd@soran.edu.iq (A.F.H.S.); ralf.arndt@fh-erfurt.de (R.W.A.); Tel.: +964-7504522250 (A.F.H.S.)

Abstract: Geopolymers can replace cement and help reduce the environmental impact of concrete construction, but research is needed to ensure their mechanical properties, durability and practicability. The aim of this investigation is to examine the influence of ground granulated blast furnace slag (slag) content on the performance, at the fresh and hardened states, of fly ash (FA) based self-compacted geopolymer concrete (SCGC). For this purpose, four SCGC mixtures containing 450 kg/m³ of total binder were examined. The alkaline-to-binder ratio was 0.5 for all mixes. FA was substituted with slag at 0%, 30%, 50%, and 100% of the total binder content. The fresh properties in terms of flowability, passing ability, viscosity, and segregation resistance, as well as the mechanical properties in terms of compressive strength and splitting tensile strength, were quantified. The durability behavior of SCGC was also studied to determine sorptivity and long-term free drying shrinkage. The results confirm that slag adversely affects the workability of SCGC mixtures except for the resistance to sieve segregation. Performance of SCGC in hardened states is in general enhanced with slag inclusion but at increased shrinkage strain. Predictions of splitting tensile strength were made using the ACI 318, ACI 363, Eurocode CEB-FIB, and Lee and Lee models. The ACI 363 and Eurocode CEB-FIB models were found to be inaccurate, except for the 30% slag mix. Predicted values obtained from the Lee and Lee model were very close to the actual values of the FA-based SCGC mix. The results of this work could lead to more sustainable concretes using geopolymers instead of OPC.

Keywords: self-compacted geopolymer concrete (SCGC); slag/fly ash; fresh properties; mechanical properties; empirical equation; sorptivity; long-term free drying shrinkage



Citation: Sherwani, A.F.H.; Younis, K.H.; Arndt, R.W.; Pilakoutas, K. Performance of Self-Compacted Geopolymer Concrete Containing Fly Ash and Slag as Binders. *Sustainability* **2022**, *14*, 15063. <https://doi.org/10.3390/su142215063>

Academic Editor: Ahmed Salih Mohammed

Received: 2 August 2022

Accepted: 1 September 2022

Published: 14 November 2022

Publisher's Note: MDPI stays neutral with regard to jurisdictional claims in published maps and institutional affiliations.



Copyright: © 2022 by the authors. Licensee MDPI, Basel, Switzerland. This article is an open access article distributed under the terms and conditions of the Creative Commons Attribution (CC BY) license (<https://creativecommons.org/licenses/by/4.0/>).

1. Introduction

Industrialization, urbanization, and population growth are the main drivers of environmental pollution and climate change and the construction industry is a major contributor. To accommodate infrastructure development, the current worldwide concrete consumption per person exceeds one cubic meter per annum [1]. Increasing demand for concrete using ordinary Portland cement (OPC) is responsible for environmental pollution, depletion of natural resources and the emission of substantial amounts of carbon dioxide (6–7% of worldwide emissions) [2,3]. Geopolymer concrete that can be made using other industrial wastes may help the concrete industry reduce its environmental impact and carbon emissions in an economical manner [4].

The term "geopolymer," was first coined in 1978 by Davidovits [5]. The polymerization process involves an aluminosilicate source material including silica (Si) and alumina (Al) and an alkaline liquid, leading to an amorphous structure. Due to its environmental

credentials, geopolymer concrete has gained popularity and attracts the interest of many scientists. Geopolymer raw materials do not require a large energy input because they are not calcined at high temperatures, a prerequisite for producing cement raw materials. It has been established that the production of geopolymers emits five to six times less carbon dioxide than Portland cement [6]. In addition, geopolymer concrete offers similar or superior fresh and mechanical properties compared to conventional concrete [7]. This type of concrete is affected by many mixed proportion parameters as well as curing conditions [8–10]. Furthermore, this type of concrete reduces energy consumption, waste disposal, and construction costs [10]. To synthesize geopolymers, it is desirable to combine fly ash (FA) with some other high silica sources, such as slag, rice husk ash, silica fume, etc. [11]. Li et al. [12] observed that slag, a by-product of iron production from blast furnace, containing calcium, magnesium silicates, and aluminosilicates, is another candidate waste product available worldwide in huge quantities. The production of one ton of slag emits just 70 kg of carbon dioxide (CO_2), which is only 7% of the CO_2 emitted during cement production. However, the use of slag in FA-based geopolymers decreases setting time and workability. Nonetheless, the calcium oxide (CaO) of slag forms calcium-silicate-hydrates (C-S-H) with aluminosilicate gel, which boosts the mechanical characteristics of concrete [13–17]. The substitution of slag with FA thus improves the initial setting time of geopolymer paste [18]. It was reported that the inclusion of slag leads to the reduction of the fresh state properties of SCGC, whilst improving the hardened state properties [19].

Self-compacted concrete (SCC) was introduced to provide optimum compaction and to help place concrete in confined spaces [20–22]. The fundamental aspects of SCC are flow, filling, and passage ability that can resist segregation [23]. Self-compacted geopolymer concrete (SCGC) is an innovation that would provide both environmental and practical benefits [24,25]. The fresh SCGC must comply with specifications recommended by the European Federation of National Associations Representing for Concrete (EFNARC) [26]. Currently, few investigations were conducted into SCGC, hence there is a need for further research to verify the efficacy of SCGC in both its fresh and hardened form and to develop materials for practical applications. To reduce costs and enhance the workability and mechanical properties of concrete, supplementary cementitious materials such as FA and slag are currently widely used in concrete [27].

Drying shrinkage is another important characteristic of concrete that needs to be examined, as it is critical for the durability and long-term serviceability of concrete structures [28]. Restrained drying shrinkage can cause cracking, and while it may not necessarily compromise the structural integrity of reinforced concrete structures, it may cause serious durability issues [29]. Research shows that drying shrinkage of oven-cured geopolymer concrete is often relatively low compared to conventional concrete. As reported by Wallah and Rangan [30], the majority of the water generated during the chemical reaction in FA-based geopolymer concrete may evaporate during the curing phase. As a result, the excess water in the hardened concrete's micropores is minimal, and thus the drying shrinkage is very limited. Other researchers also confirm that conventionally cured geopolymer concrete made from FA has good engineering performance and low drying shrinkage [31,32]. However, Wang et al. [33] showed that slag-based geopolymer concretes activated with sodium silicate might result in higher shrinkage strains than OPC concrete due to the development of silica-rich gel. For this reason, the long-term free drying shrinkage of FA-based SCGC made with/without slag needs to be examined.

Details of the binder type used and investigated properties of previous research on plain SCGC made with/without FA and slag are summarized in Table 1. Details of the current investigation are also displayed at the bottom of Table 1.

Table 1. Details of binder type used and examined properties of SCGC in the previous research and current study.

Refs	Binder Type	Fresh Properties	Mechanical Properties	Durability Properties	Others
[34]	FA (100,75,50,25,0%) slag (0,25,50,75,100%)	Slump, T ₅₀₀ and V-funnel flow time, L-box height	Compressive, splitting, fracture parameters	-	Statistical Evaluation, correlation
[35]	FA (50%), slag (50%), NS ¹ (5–10 kg/m ³)	Slump, T ₅₀₀ and V-funnel flow time, L-box height	Compressive, fracture parameters, bond strength,	-	Statistical Evaluation, correlation
[36]	FA (25%), slag (75%)	Slump, T ₅₀₀ and V-funnel flow time, L-box and J-ring height, U-box	Compressive	Rapid chloride and water permeability, Sorptivity, Abrasion, Acid and sulphate attack, shrinkage	
[37]	slag, NS (9–10 kg/m ³)	Slump, T ₅₀₀ and V-funnel flow time, and J-ring height	Compressive, flexural, bond strength	Sorptivity	XRD
[38]	FA (Class F & C)	Slump, T ₅₀₀ flow time, L-box height, U-box	Compressive	Rapid chloride permeability, Sorptivity, Acid and sulphate attack, corrosion	SEM
[4]	FA (100%), slag (100,95,85, 75%), RHA ² (5, 15, 25%)	Slump, T ₅₀₀ and V-funnel flow time, L-box and J-ring height	Compressive, splitting, flexural	Sorptivity	SEM
[39]	FA (100%), slag (100,95,85, 75%), RHA (5, 15, 25%)	Slump, T ₅₀₀ and V-funnel flow time, L-box and J-ring height	Compressive, splitting, flexural	-	SEM
[40]	FA	Slump, V-funnel flow time, L-box height	Compressive, splitting	Water absorption	
[24]	FA	Slump, T ₅₀₀ and V-funnel flow time, L-box and J-ring height	Compressive	-	-
[41]	FA	Slump, T ₅₀₀ and V-funnel flow time, L-box and J-ring height	Compressive	-	-
[42]	FA	Slump, T ₅₀₀ and V-funnel flow time, L-box and J-ring height	Compressive	-	SEM
[43]	FA (100,80,60,40,20,0%) , slag (100,80,60,40,20,0%)	Slump, T ₅₀₀ and V-funnel flow time, L-box height	Compressive, splitting, flexural	-	-
[25]	FA	Slump, T ₅₀₀ and V-funnel flow time, L-box and J-ring height, sieve segregation	Compressive	-	-
[44]	FA (100,95,90,85,80%) MK ³ (5,10,15,20%) GSA ⁴ (5,10,15,20%)	Slump, T ₅₀₀ and V-funnel flow time, L-box and J-ring height	Compressive, splitting, flexural	Water permeability	-
[45]	MK	-	Flexural strength	Water absorption Carbonation depth, drying shrinkage, acid resistance, water absorption,	SEM
[46]	slag	Slump, T ₅₀₀ and V-funnel flow time, L-box height	Compressive, splitting, flexural		SEM
[47]	FA	Slump, T ₅₀₀ and V-funnel flow time, J-ring height	Compressive, splitting, flexural strength	-	-
[48]	FA (50%), slag (50%)	Slump, T ₅₀₀ and V-funnel flow time, L-box height	Compressive	-	-
[49]	FA (100–70%), slag (10,20,30%), SF ⁵ (5,10,15%)	Slump, T ₅₀₀ and V-funnel flow time, L-box height, U-box	Compressive, splitting, flexural strength	-	-
[50]	Slag (100, 98%), NS (2%)	Slump, T ₅₀₀ and V-funnel flow time, L-box height	Compressive, splitting, fracture parameters, modulus of elasticity	-	-

Table 1. Cont.

Refs	Binder Type	Fresh Properties	Mechanical Properties	Durability Properties	Others
[51]	FA	Slump, T ₅₀₀ and V-funnel flow time, L-box and J-ring height	Compressive	-	-
[52]	FA (100,90,80,70%), MK (10,20,30%)	Slump, T ₅₀₀ and V-funnel flow time, L-box height	Compressive, splitting, flexural	-	-
[32]	FA (100,90%), SF (10%)	-	-	Shrinkage	-
[53]	Slag (100,70,60,50,40,30%)FA (30,40,50,60,70%)	Slump, T ₅₀₀ and V-funnel flow time, L-box and J-ring height	Compressive, splitting, flexural	-	XRD, SEM, correlation, modeling
The current study	FA (100,70,50,0%) slag (0,30,50,100%)	Slump and J-ring flow, T ₅₀₀ , T _{J500} , and V-funnel flow time, L-box and J-ring height sieve segregation	Compressive, splitting	Sorptivity, long-term free drying shrinkage, long-term mass loss	Correlation, an empirical equation

Where ¹ NS is nano-silica, ² RHA is rice husk ash, ³ MK is metakaolin, ⁴ GSA is groundnut shell ash, ⁵ SF is silica fume.

Studies on the influence of slag content on fresh, mechanical, and durability behaviors, as well as mechanical property predictive models, are limited. The study presented here aims at filling these gaps by examining the impact of slag inclusion on the various fresh, mechanical, and durability properties of FA-based SCGC specimens. Slump flow, T₅₀₀, J-ring flow, T_{J500}, J-ring height, L-box, V-funnel, and sieve segregation resistance are the fresh property tests to be used in this work. In terms of mechanical properties, both the compressive and splitting tensile strength will be determined. In terms of durability, sorptivity and long-term free drying shrinkage will be investigated. Correlations between different properties will be attempted and comparisons with existing predictive models made.

2. Materials

Class F fly ash (FA) and ground granulated blast furnace slag (slag) were utilized as a binder. Their chemical and physical features are presented in Table 2.

Table 2. Chemical and physical features of FA and slag in the presented study.

Component %	CaO	SiO ₂	Al ₂ O ₃	Fe ₂ O ₃	MgO	Various	Specific Gravity	Loss on Ignition	Blain Fineness (cm ² /g)
FA	4.0	56	24	7.0	2.0	7.0	2.28	3.0	3098
Slag	40	36	11	0.4	7.6	5.0	2.80	2.3	4250

The alkaline activator utilized in this study was a blend of sodium silicate (Na₂SiO₃) and sodium hydroxide (NaOH). The alkaline/binder ratio was kept at 0.5 in this study, the molarity (M) constant at 12, and the Na₂SiO₃/NaOH ratio at 2.5 [34]. The mass of Na₂SiO₃ used in the production of SCGC was 45% dry (of which 15% was Na₂O and 30% SiO₂) and 55% water content. The NaOH was 99% pure. The NaOH solution was made by dissolving solid NaOH pellets in water, targeting at 12 M molarity.

Coarse and fine natural aggregates used in this study were gravel and sand, respectively. The physical features of the used aggregates are shown in Table 3.

Table 3. Physical features of gravel and sand in the presented study.

Type of FA	Size (mm)	Specific Gravity	Water Absorption (%)
Gravel	4–16	2.70	0.5
Sand	0–4	2.66	0.8
Standard	BS EN 933-1+ A1 2005 [54]	BS EN 1097-6:2013 [55]	BS EN 1097-6:2013 [55]

The superplasticizer (SP) used was MC Power flow evo 502, a SP based on polycarboxylate ether that meets the standards of EN 934-2: T3.1/3.2. It is a fifth generation MC-superplasticizer with improved rheological properties. It is yellow in color and has a density of 1.03 kg/m³. Tap water content was maintained at 40 kg/m³ throughout the research.

3. Mixing Procedure

Four SCGC mixtures were prepared with 450 kg/m³ total binder content [35]. Different amounts of slag were used to make these combinations, while the other parts remained constant. Slag was used in this study to replace the FA at 0%, 30%, 50%, and 100% replacement levels. Table 4 shows the detailed mix proportions. In the following mix codes, G% denotes the slag percentage used.

Table 4. Mix proportions of SCGC in the presented study.

Mix Code	Binder (kg/m ³)	FA (%)	Slag (%)	Gravel (kg/m ³)	Sand (kg/m ³)	Alkaline/Binder	Molarity (M)	SP (%)	Water (kg/m ³)
G0	450	100	0	800	825	0.5	12	7	40
G30		70	30						
G50		50	50						
G100		100	100						

3.1. Mixing and Casting

A comparable mixing process was employed to attain consistency and homogeneity in each mixture. In the first phase, the dry ingredients, including aggregates (gravel and sand), and binder (FA and slag), were blended for approximately 2 min in an electric concrete mixer with a 75-L capacity. After properly blending the dry ingredients, the blended liquids of alkaline activator and water were fed to the mixer and wet mixed for two more minutes. The superplasticizer was added to the wet batch, and mixing proceeded for an extra two minutes. After the mixing process was completed, SCGC mixtures were tested in their fresh state, and then samples for hardened state characteristics were cast. Before placing the concrete into the molds, the fresh concrete was re-mixed in the mixer for thirty seconds to ensure the homogeneity of the mixture.

3.2. Curing Method

The samples were kept for 24 h in the laboratory [56] prior to being oven-cured at 85 °C for 24 h, except for the shrinkage tests. It should be noted that the SCGC specimens made with 100% FA (G0) did not harden enough after 24 h due to the low content of CaO, which is considered the main compound that affects the initial setting time of concrete. Slag can be added to the FA-based SCGC to enhance the setting time [34]. Therefore, in this study, the geopolymer concrete specimens were subjected to heat-curing after one day without being removed from the molds. After oven curing, the hardened samples were stored at ambient temperature until the testing date.

4. Testing Procedure

4.1. Fresh Properties

The flowability of the SCGC mixtures were evaluated using slump flow, J-ring flow, and V-funnel tests, passing-ability was assessed through the use of the L-box and J-ring height tests, and viscosity was evaluated via V-funnel, T_{500 mm}, and TJ_{500 mm}, according to the EFNARC recommendations [57]. Segregation resistance was measured via a sieve segregation test [58]. The J-ring test is a combination test to assess the filling-and-passing-ability of the freshly mixed SCGC through a restricted and congested area without blocking. During this test, J-ring flow diameter, TJ_{500 mm}, and J-ring height were calculated.

Figure 1 shows photos of the fresh tests conducted in this study. Flow diameters in the x and y directions were monitored in the slump flow and J-ring flow tests, and the $T_{500\text{ mm}}$ and $TJ_{500\text{ mm}}$ flow times at which the flow diameter reached 500 mm were also recorded. The J-ring height, or passing ability (PJ), which refers to the blocking of fresh concrete through congested reinforcement bars, was measured once the concrete flow had stopped moving. Then, in the center of the J-ring, the straight rod was placed with its flat side down and to measure the distance (in mm) between the lower edge of the rod and the concrete surface (h_o). Following that, the height (mm) of four spots outside the J-ring, two along the x-axis ($hx1$, $hx2$) and two along the y-axis ($hy1$, $hy2$) were measured. The following equation was used to determine the PJ value in mm:

$$PJ = \frac{hx1 + hx2 + hy1 + hy2}{4} - h_o \quad (1)$$

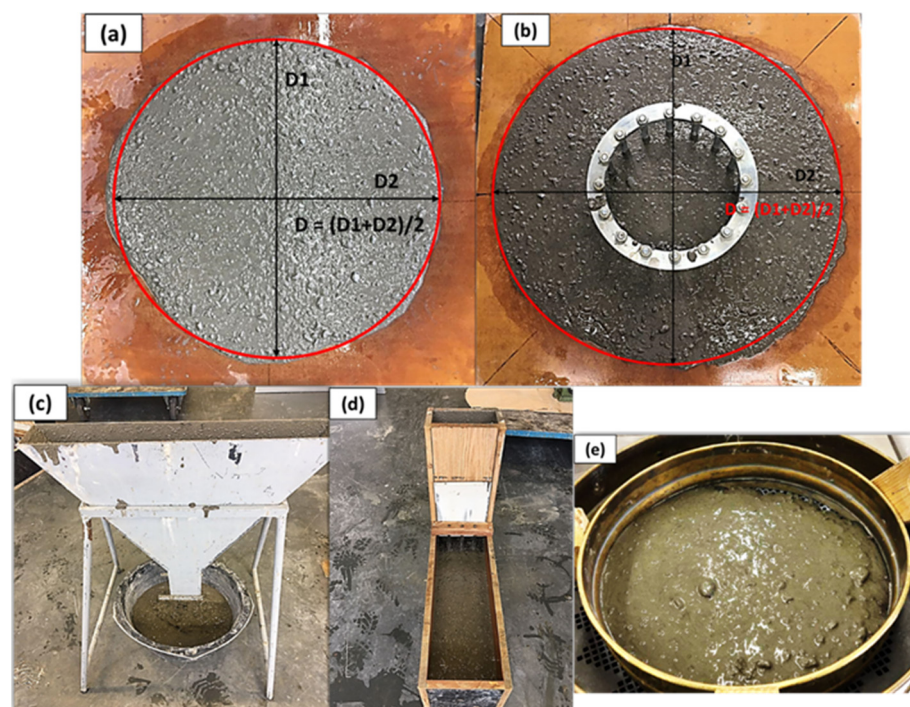


Figure 1. Fresh test apparatus: (a) slump test, (b) J-ring test, (c) V-funnel test, (d) L-box test, and (e) sieve segregation test.

The V-funnel test involves completely filling the V-shaped section with concrete, allowing the concrete to discharge, and recording the discharge time. The concrete viscosity in its fresh condition can be assessed indirectly using the V-funnel flow time and $T_{500\text{ mm}}$ test measurements, as well as the V-funnel and $TJ_{500\text{ mm}}$ test records. The SCGC's passing-ability (PA) between tiny gaps of bars was determined by means of the L-box test by dividing the horizontal section's concrete height by the vertical section's height after the concrete flow has stopped. The sieve segregation test was conducted using a sieve having 5 mm holes, a 300 mm diameter, and a 30 mm height. After finishing the mixing process, approximately 5 kg of the fresh concrete was placed in a plastic container and set aside for 15 min. The pan was then weighed dry (m_p). After that, a sieve and pan were placed on the scale and approximately 4.8 kg of fresh SCGC was carefully placed at half a meter height, and the weight was recorded (m_s). After two minutes, the sieve was carefully lifted, and the amount of concrete that had passed through the 5 mm holes and remained in the pan were weighed (m_{ps}). The sieve segregation index (SI) was calculated using the following equation:

$$SI, \% = \frac{(m_{ps} - m_p) * 100}{m_s} \quad (2)$$

Table 5 Displays the upper and lower bounds that EFNARC has established for the performance of SCC mixtures in their fresh state [57].

Table 5. Fresh test assessment following the EFNARC guidelines.

Flowability Classes			
Classes	Slump Flow and J-Ring Flow Diameter (mm)		
Slump flow (SF) 1	550–650		
Slump flow (SF) 2	660–750		
Slump flow (SF) 3	760–850		
Viscosity Classes			
Class	T ₅₀₀ (sec)	TJ ₅₀₀ (sec)	V-Funnel time (sec)
Viscosity (VS1/VF1)	≤2	≤2	≤8
Viscosity (VS2/VF2)	>2 and ≤5	>2 and ≤6	9 to 25
Passing ability			
Classes	J-Ring passing ability		
Passing-ability (PJ) 1	≤10 mm		
Passing-ability (PJ) 2	≥10, 20 mm		
Classes	L-Box height ratio		
Passing-ability (PA) 1	≥0.8 with two rebar		
Passing-ability (PA) 2	≥0.8 with three rebar		
Segregation resistance [58]			
Classes	Sieve segregation resistance (%)		
SI 1	≤20%		
SI 2	≤15%		

4.2. Mechanical Properties

The compressive strength of hardened SCGC specimens was obtained at 7 and 28 days of age from three 100 mm cube according to BS EN 12390 [59]. The splitting tensile strength was determined according to BS EN 12390-6 [60] using the average of three cylindrical samples of Ø150 × 300 mm at 28 days of age.

4.3. Correlation between Splitting Tensile and Compressive Strength

Normally, there is a good correlation between the mechanical properties of concrete (compressive strength, elastic modulus and tensile/flexural/splitting strength). Hence, the 28 day splitting tensile strength can be predicted from the compressive strength using empirical equations proposed by ACI 318-11 [61], ACI 363R-10 [62], CEB-FIB [63], and Lee and Lee [64], as tabulated in Table 6. The empirical equations provided by codes and literature are based on the cylindrical compressive strength values f_c in MPa. As cubes were tested in this study the following conversion equation was used [65]:

$$f_c = 0.8 \times f_{cu} \quad (3)$$

where 0.8 is the conversion factor.

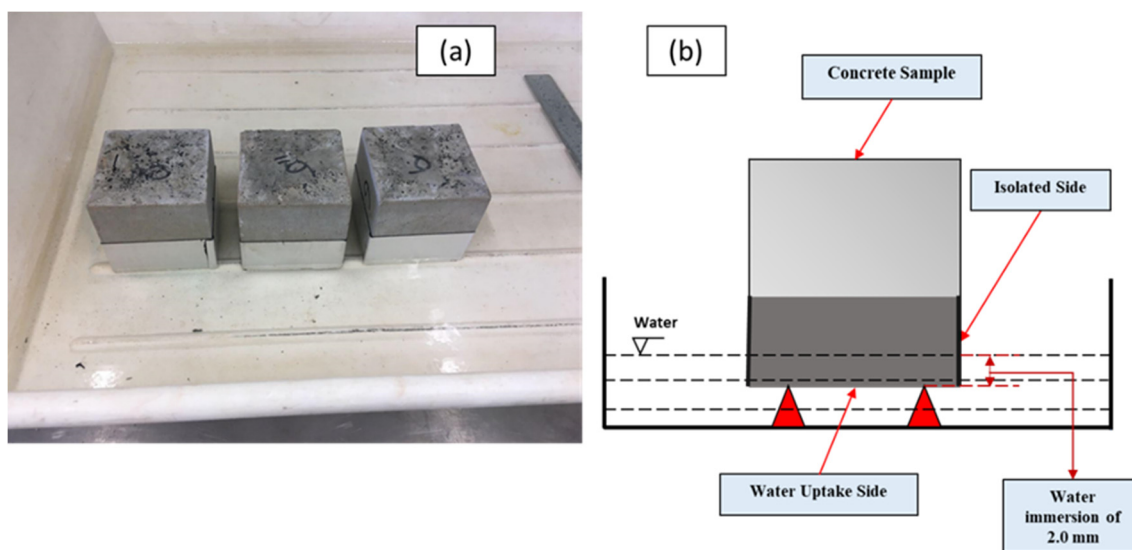
Table 6. ACI predictive equations for the splitting tensile strength of concrete.

Property	Standard	Equation	
Splitting Tensile Strength, f_t (MPa)	ACI 318 [61]	$f_t = 0.56\sqrt{f}$	(4)
	ACI 363 [62]	$f_t = 0.59\sqrt{f}$ for 21 MPa < f_c < 83 MPa	(5)
	CEB-FIB [63]	$f_t = 0.3f_c^{2/3}$	(6)
	Lee and Lee [64]	$f_t = 0.45\sqrt{f}$	(7)

4.4. Durability Properties

4.4.1. Capillary Water Absorption (Sorptivity)

The rate of water absorption per unit area was measured from the capillary water absorption of three 100 mm cubes. After 28 days, the specimens' sides were taped to prevent water absorption from the sides. The specimens were then placed on a tray and rested on knife-edge supports to obtain a depth of water immersion of 2.0 mm, in accordance with BS EN 13057 [66] (see Figure 2). The mass resulting from water absorption from the bottom surface was determined over time (0 min, 12 min, 30 min, 60 min, 120 min, 240 min, and 1440 min). The water uptake was determined by plotting the weight gain per unit area against the square root of time, and the slope of the best fit line was used to calculate the Sorptivity coefficient (index) [67,68].

**Figure 2.** Capillary absorption test: (a) specimen set up, (b) schematic representation of specimens.

4.4.2. Free Drying Shrinkage

To quantify drying shrinkage and mass loss of SCGC, two 100 × 100 × 300 mm prisms were used for the G0 and G50 mixes according to ASTM C 157 [69]. After casting, the prisms were left at ambient conditions for 24 h, then exposed to oven curing at 40 °C for three days [70]. Following curing, the prisms were demolded, and demec points were glued to the specimens at a gauge length of 200 mm mid-height on two sides (see Figure 3). The change in length was determined by a dial gauge extensometer, with a strain accuracy of 5 µε (see Figure 4). Initial measurements of length and weight were carefully recorded. The prisms were then placed in a controlled climate chamber and subjected to a drying condition (22 ± 2 °C and 50 ± 2% relative humidity (RH)). Measurements of length and weight were taken over a period of a year; every 24 h for the first week, four times a week for the later three weeks, once per week for the second month, once per two weeks for the

third month, and then once per month for the long-term periods (six, nine, and 12 months). The values were averaged for the two samples.

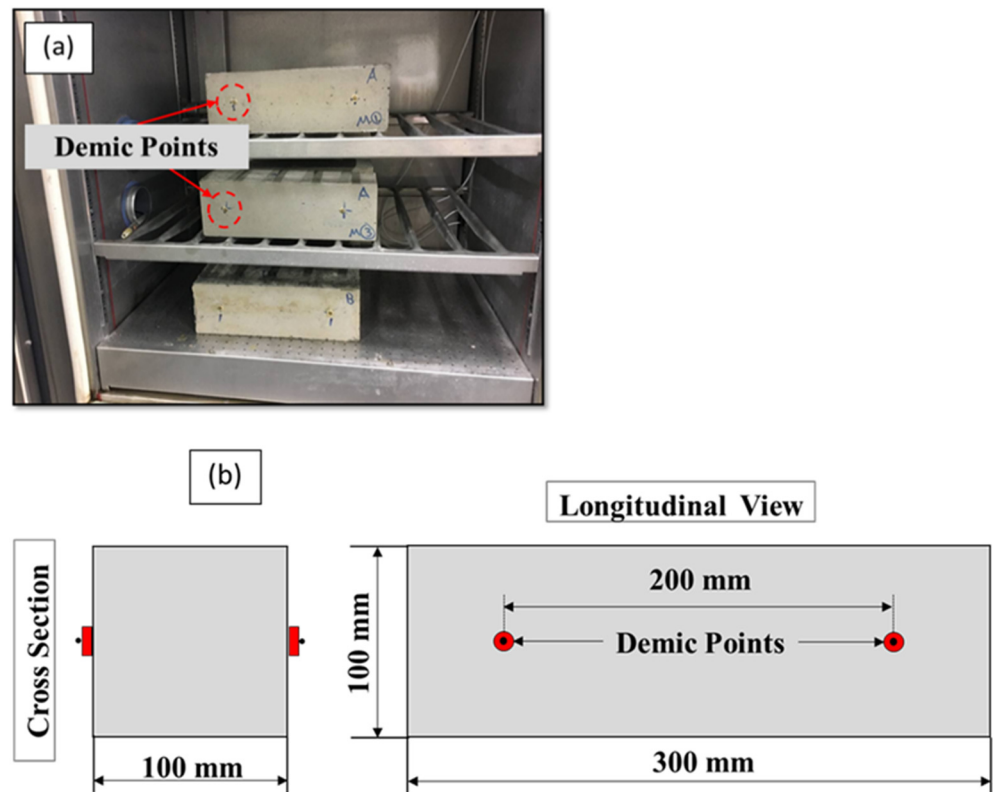


Figure 3. Free drying shrinkage test: (a) prisms are placed in a controlled climate chamber, (b) geometry of the specimens.

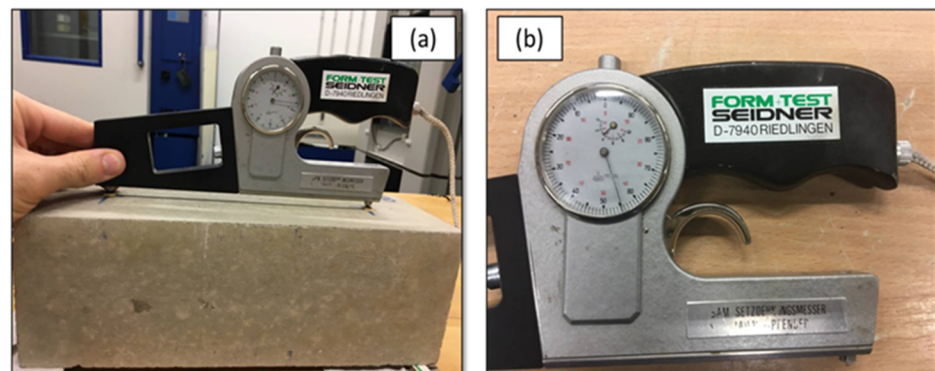


Figure 4. Free drying shrinkage measurement: (a) specimen measurement, (b) strain gauge measurement device developed by BAM.

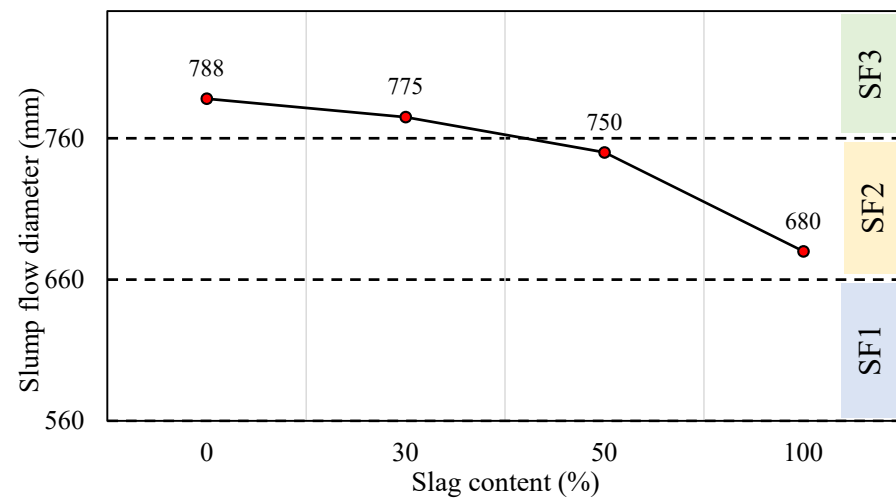
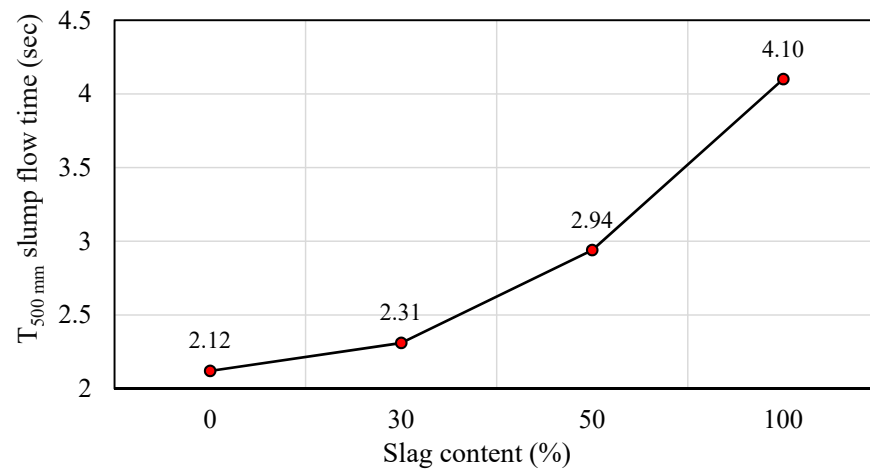
5. Result and Discussion

5.1. Fresh Properties

The impact of utilizing slag as a binder on the performance of FA based SCGC mixes was investigated, and the results were compared with the limits of EFNARC [57]. The results of the fresh properties of SCGC mixtures with various slag contents are presented in Table 7 and Figures 5–18.

Table 7. Fresh test results of the SCGC in the presented study.

Mix Code	Slag (%)	Slump (mm)	J-Ring (mm)	T ₅₀₀ (s)	TJ ₅₀₀ (sec)	PJ (mm)	V-Funnel (s)	L-Box	Segregation Index (%)
G0	0	788	780	2.12	2.42	0.0	7.5	1.00	28.7
G30	30	775	760	2.31	2.71	1.0	10.3	0.99	22.4
G50	50	750	738	2.94	3.31	2.7	12.0	0.96	18.4
G100	100	680	665	4.10	4.43	7.1	17.1	0.84	11.4

**Figure 5.** Influence of slag content on the slump results.**Figure 6.** Influence of slag content on the T500 mm flow time.

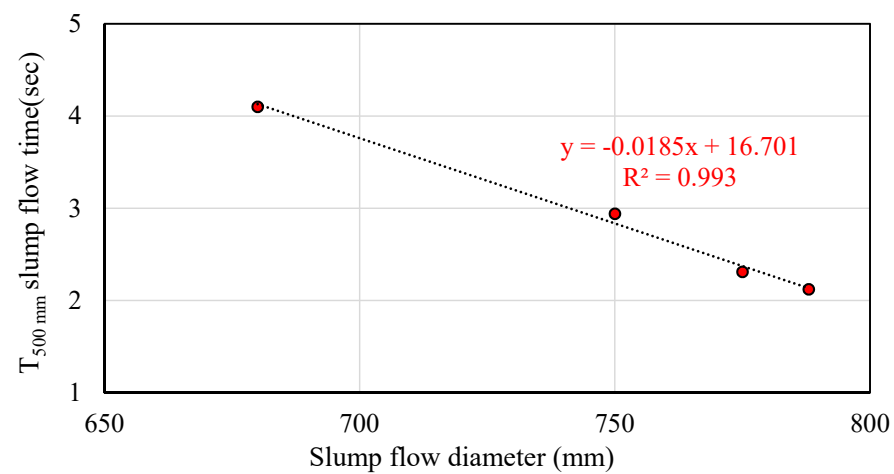


Figure 7. Correlation between $T_{500\text{ mm}}$ slump flow time and slump flow diameter.

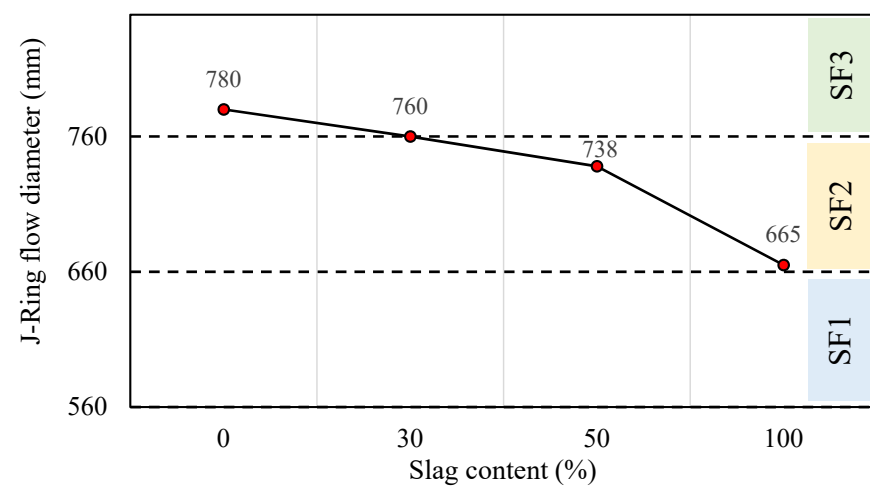


Figure 8. Influence of slag content on the J-ring flow diameter.

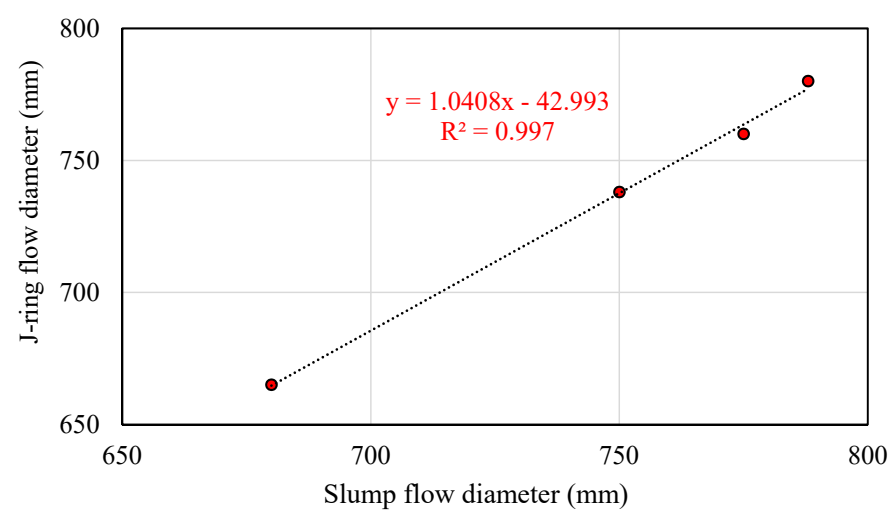


Figure 9. Correlation between J-ring and slump flow diameter.

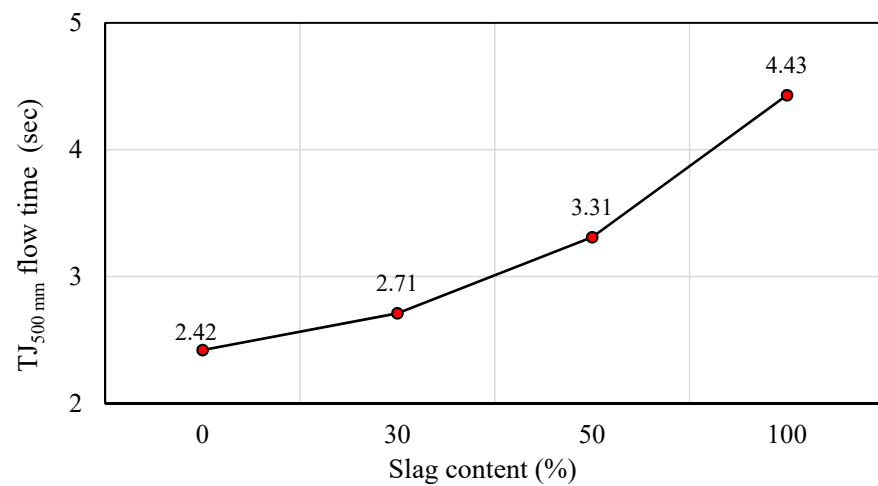


Figure 10. Influence of slag content on the TJ_{500 mm} flow time.

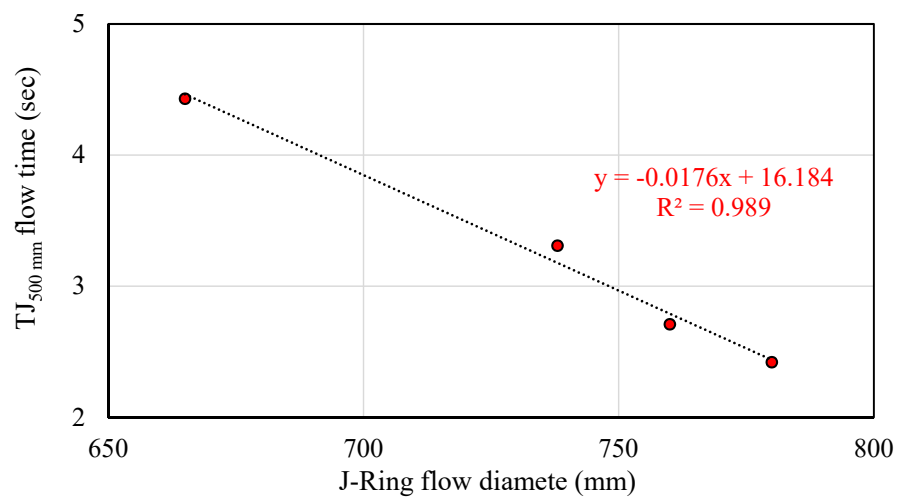


Figure 11. Correlation between TJ_{500 mm} slump flow time and J-ring flow diameter.

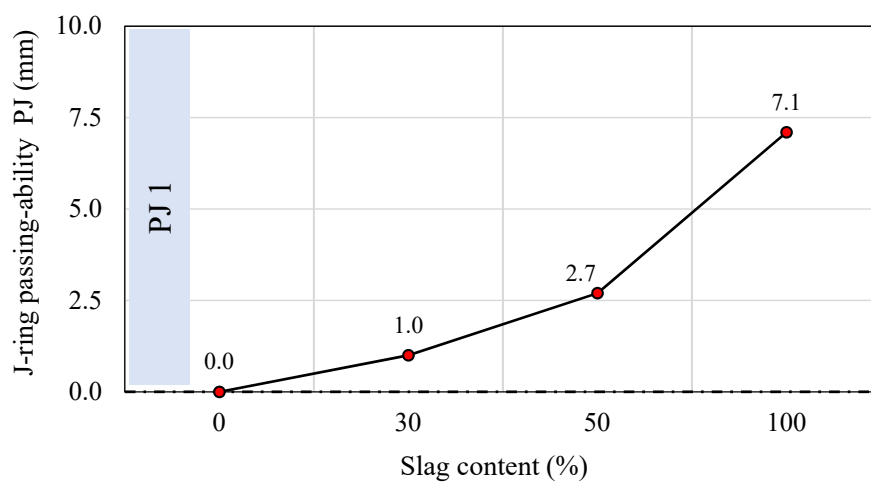


Figure 12. Influence of slag content on the J-ring passing-ability.

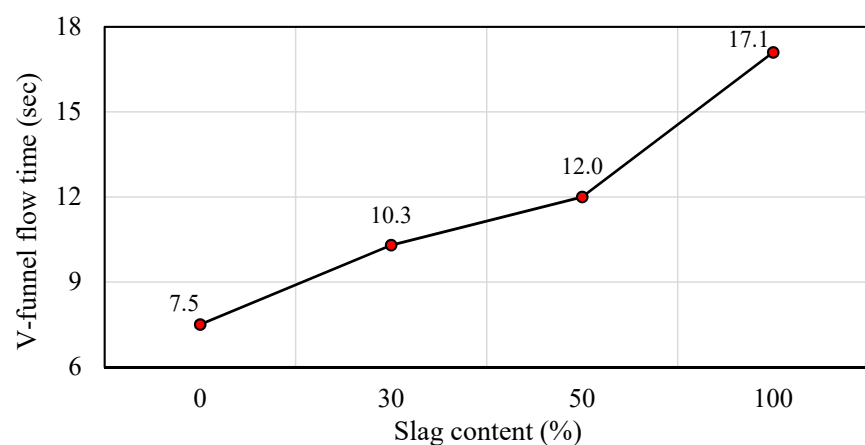


Figure 13. Influence of slag content on the V-funnel flow time.

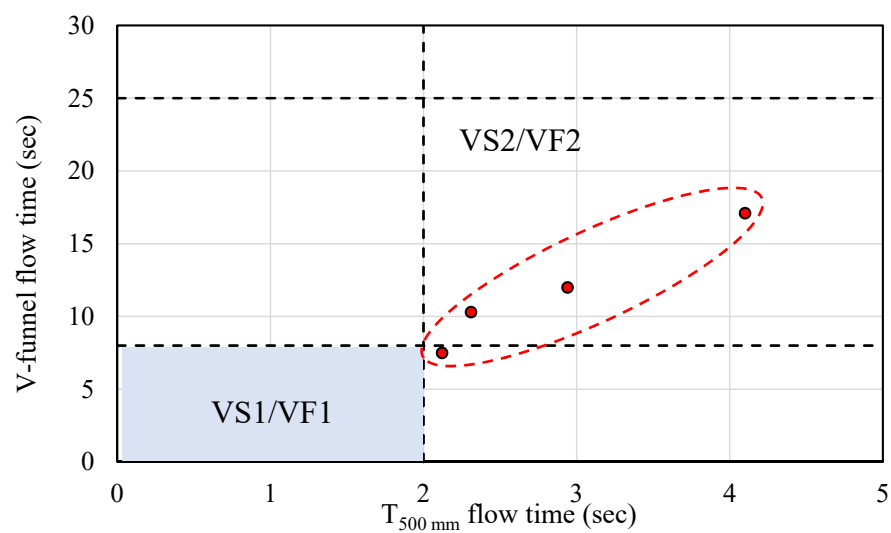


Figure 14. Viscosity class variation with V-funnel and $T_{500\text{ mm}}$.

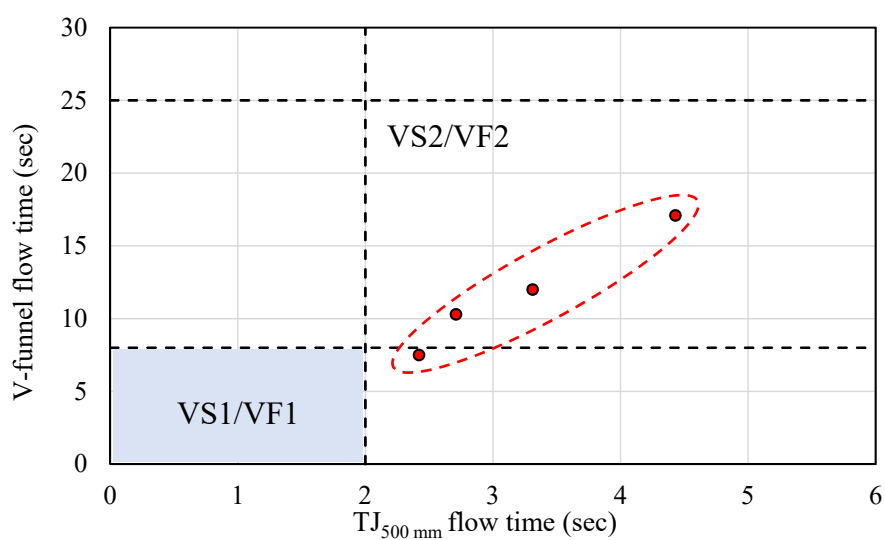


Figure 15. Viscosity class variation with V-funnel and $TJ_{500\text{ mm}}$.

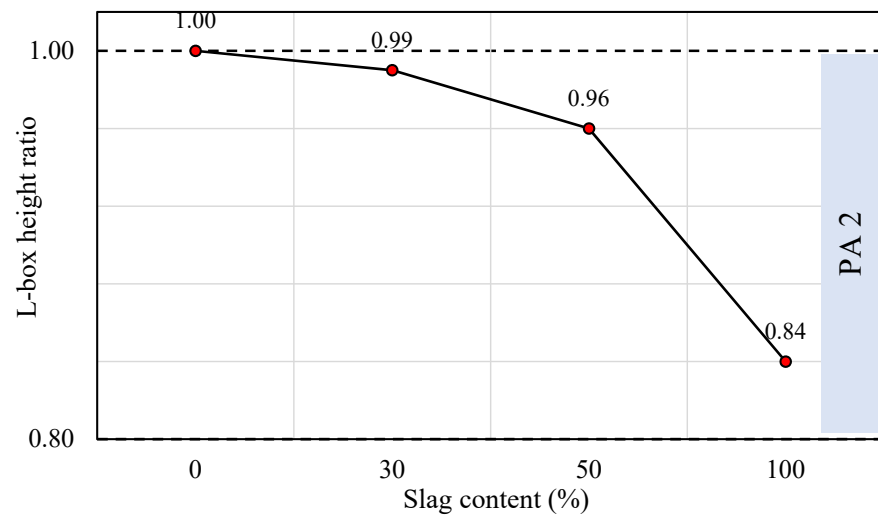


Figure 16. Influence of slag content on the L-box height ratio.

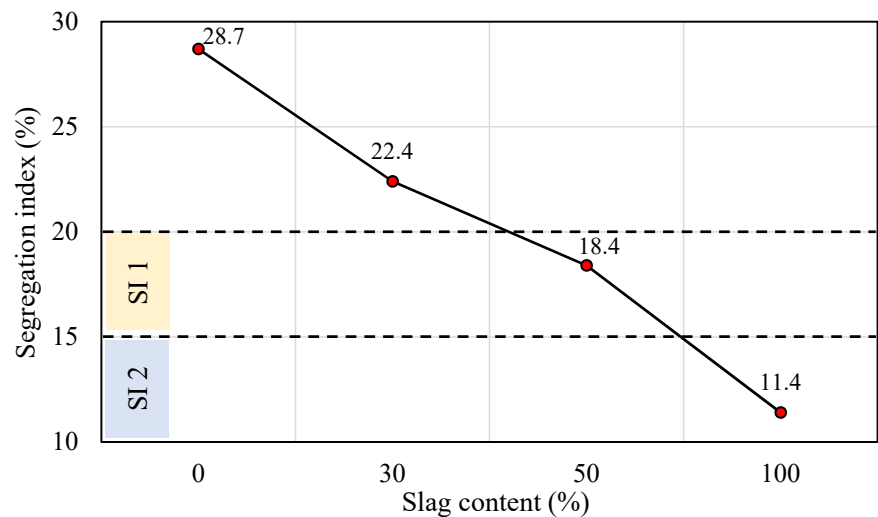


Figure 17. Influence of slag content on the segregation index.

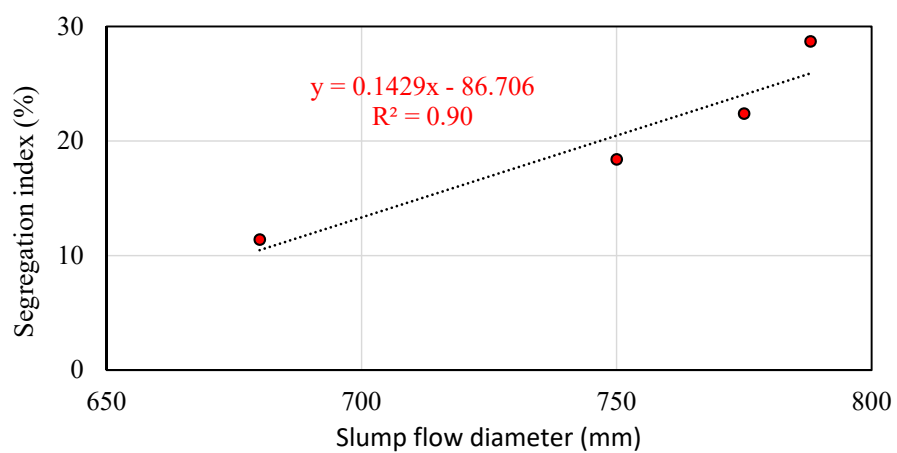


Figure 18. Correlation between segregation index and slump flow diameter.

5.1.1. Slump Flow Diameter

The slump flow diameter values of the produced geopolymer concrete in mm with respect to the slag content are shown in Figure 5. The slump values range from 788 to

680 mm, showing a systematic decrease with the increase in slag content. This is because slag binders have a larger specific surface area than FA binders, which demands a higher quantity of mixing water, thereby diminishing the workability of the freshly mixed concrete.

The slump flow values for the produced SCGCs of the mixes, including 0% and 30% slag content are in the range of the SF3 class, and the mixes containing 50% and 100% slag content in the range of the SF2 class of EFNARC limits. Based on the EFNARC limitations [57], the SF2 class can be used for constructions with complex geometries, vertical applications, and filling beneath the formwork. However, SCGC in the SF3 class provides a better surface finish than SCGC in the SF2 class. On the other hand, controlling segregation resistance is more difficult in the SF3 class. Previous studies recorded values between 755 and 650 mm for the blended fly ash and slag blended SCGC [34]. Moreover, the results align with the BS EN 12350-8 standard [71] which specifies that slump values should have an average diameter greater than 600 mm.

5.1.2. $T_{500\text{ mm}}$ Slump Flow Time

Figure 6 shows the influence of slag on the $T_{500\text{ mm}}$ slump flow time, in which time is measured up to the point at which the flow diameter of the freshly mixed concrete reaches 500 mm. In the results of T_{500} , it can be observed that by increasing the slag content, the slump flow time is increased. The recorded $T_{500\text{ mm}}$ slump flow in this study was between 2.12 and 4.10 s. $T_{500\text{ mm}}$ meet the requirements of the EFNARC specifications [57] and the BS EN 12350-8 standard (less than 6 s) [71].

To examine the correlation between these two tests, the inverse linear relationship between flow time and flow diameter data is depicted in Figure 7. The R-square value of 0.993 shows a strong correlation between the T_{500} and Slump flow diameter values of the mixes conducted in this study.

5.1.3. J-Ring Flow Diameter

The J-ring flow diameter test is used to determine the flow spread of the fresh mixed SCC as it flows through the J-ring. In this test, the J-ring flow diameter in mm for the various slag content is evaluated, as shown in Figure 8. It can be seen that the J-ring flow diameter decreases with the increase in slag content. The J-ring results ranged between 780 and 665 mm for the slag contents of 0% and 100%, respectively. The mixes of the SCGC can be classified into the SF3 class when the slag content ratio ranges between (0 to 30%) and the SF2 class when the slag content ratio exceeds 30% up to 100%. The test values are within the EFNARC limits [57]. Furthermore, the linear correlation between J-ring and slump flow diameter is found in Figure 9. From the figure, the R-square is 0.997, indicating a strong relationship between J-ring-and-slump flow diameter outcomes. This means that both results are proportional to the slag content. Safiuddin et al. [72], who studied the fresh properties of SCC and achieved a 0.998 correlation coefficient between J-ring and slump flow diameter, also confirmed this result.

5.1.4. $TJ_{500\text{ mm}}$ Flow Time

The $TJ_{500\text{ mm}}$ flow time outcomes of the SCGC with different slag content are shown in Table 7 and Figure 10. The flow time measured for the $TJ_{500\text{ mm}}$ test varies between 2.42 and 4.43 s. According to EFNARC specifications and guidelines [57], the $TJ_{500\text{ mm}}$ of SCC typically takes between 2 and 6 sec. Hence, the $TJ_{500\text{ mm}}$ values are within a satisfactory range. The influence of slag content on the $TJ_{500\text{ mm}}$ of SCGC is obvious from Figure 10, and the $TJ_{500\text{ mm}}$ results decreased with the increase in slag content. Moreover, the correlation coefficient (R-square) for the $TJ_{500\text{ mm}}$ slump flow time and J-ring flow diameter is depicted in Figure 11. The R^2 of 0.989 shows a very strong relationship between $TJ_{500\text{ mm}}$ flow time via J-ring flow diameter. As expected, there is an inverse linear relationship between the two measurements.

5.1.5. J-Ring Passing-Ability

The J-ring passing ability values with respect to slag content are illustrated in Figure 12. It can be seen that the passing-ability increases with the inclusion of slag. The test values were located between 0.0 and 7.1 mm for the slag content of 0% and 100%, respectively. According to the EFNARC specifications [57], the J-ring passing-ability for values smaller than 10 mm is classed as PJ 1. Therefore, the PJ values are typically in the range of PJ 1 class for the mixes in the study, with values less than 10 mm, which indicates good passing ability.

5.1.6. V-Funnel Flow Time

The discharge time from the V-funnel flow time test is comparable to the slump flow test results, as depicted in Figure 13. The test values increase with increasing slag content. The EFNARC requirements [57] specify viscosity classes based on V-funnel, $T_{500\text{ mm}}$ slump, and $TJ_{500\text{ mm}}$ slump flow time test results, as can be seen in Table 7. In addition, the viscosity class variations between V-funnel vs. $T_{500\text{ mm}}$ are illustrated in Figure 14. According to the test findings, all mixtures belong to the VS2/VF2 viscosity category, except for the mix created without slag (G0), which is within the VS1/VF1 viscosity class based on the V-funnel results, whereas the G0 is classified as VS2/VF2 referring to the $T_{500\text{ mm}}$ outcomes. According to EFNARC, the VS1/VF1 viscosity category has a high filling capacity, even with dense reinforcements, with a tendency to bleeding and segregation. The viscosity class VS2/VF2 offers excellent resistance to segregation. However, the VS2/VF2 class has an inadequate smooth surface texture and may be susceptible to SCGC mix flow stoppage. The results show that increasing the slag level increases the flow duration, which is advantageous for avoiding segregation and bleeding but may result in insufficient filling ability. The EN 12350-9 [73] standard also specifies that the V-funnel outcome should be less than 15 sec to ensure adequate filling capacity. Likewise, as illustrated in Figure 15, a similar trend can be observed for the viscosity class variances between V-funnel and $TJ_{500\text{ mm}}$ flow time data.

5.1.7. L-Box Height Ratio

The L-box test determines the mixes' capacity to pass through three-bar restricted openings. The test values of SCGC mixtures should be between 0.8 and 1.0 to confirm certain passing abilities according to the EFNARC guidelines [57] and the EN12350-10 standard [71]. From the test results presented in Figure 16, it is feasible to ascertain that all mixtures possess an appropriate passing capacity (passing-ability > 0.8), and the L-box values are classified in the class of passing ability 2. The highest passing ability of 1.00 is for the mixes without slag content. Then, the L-box values decrease as the slag content increases.

5.1.8. Sieve Segregation

The segregation index (%) is depicted in Figure 17. With increased slag content, the segregation index begins to diminish. This is due to the fact that slag has a larger specific surface area than FA. The test values achieved in the mixes mentioned above range from 11.4% to 28.7%. Based on BS EN12350-11 [58], the segregation index should be lower than 20%. This means that the mixes with 0% and 30% slag content are out of the allowable range, whereas the mixes with 50% and 100% slag content satisfy the SI 1 and SI 2 classes, respectively. Figure 18 depicts the relationship with both the segregation index and the slump flow diameter. It can be seen that the segregation index and slump flow of the SCC mixtures have a significant linear relationship. The correlation coefficient R-square value is 0.90, indicating a significant correlation.

5.2. Mechanical Properties

Table 8 shows the results for the different mechanical properties. The SCGC specimens were cured at 85 °C for 24 h and then kept at room temperature until they reached 28 days of age. As expected, increasing the slag content of the geopolymers concrete was found to enhance the compressive strength [34].

Table 8. Hardened properties of SCGC in the presented study.

Mix Code	Slag Content (%)	Compressive (MPa)		Splitting Tensile (MPa)
		7 Days	28 Days	
G0	0	38.70	44.21	2.51
G30	30	58.17	65.72	4.31
G50	50	76.63	81.67	5.35
G100	100	80.92	85.10	5.60

5.2.1. Compressive Strength (f_{cu})

Figure 19 shows the impact of the slag content on the compressive strength of SCGC. The FA-based geopolymer concrete mixes yield the lowest strength values, whereas the inclusion of slag significantly increases the compressive strength of SCGC. The compressive strength of the seven-day-old specimens were between 38.7–80.9 MPa for the G0 and G100 mixtures, respectively. These findings are line with a study by Al-Rawi and Tayşi [34]. The compressive strength values at 28 days are very close to those at seven days of age. This may be due to the high early age development rate of geopolymer concrete due to heat curing compared to normal concrete, as has been reported by previous studies [74].

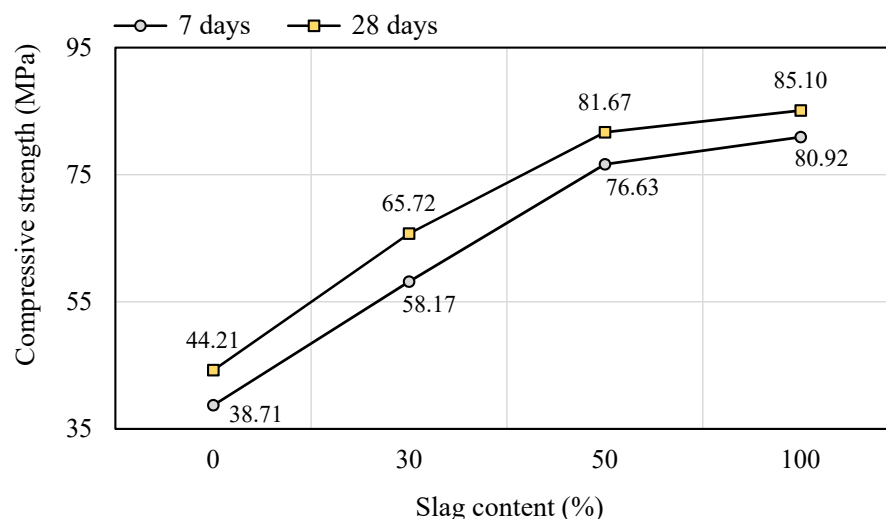
**Figure 19.** Influence of slag content on the compressive strength at seven and 28 days.

Figure 20 shows the percentage relative increase in compressive strength for the various slag content compared to the mix without slag. At 7 days, the improvement in strength of SCGC was 98.0% and 109.0%, for the slag contents 50%, and 100%, respectively. The results confirm that the biggest increase in strength comes with the replacement of 50% slag.

The effect of slag, FA, and blended FA and slag binders on the compressive strength of OPC and geopolymer mortars was also examined by Chi and Huang [75]. The results showed that the compressive strength of geopolymer mortars (excluding FA-based geopolymer mortars) was higher than that of ordinary Portland cement mortars. During X-Ray Diffraction tests, specimens containing 100% FA reveal a low rate of reactive calcium, resulting in a low level of C-S-H. As a result, specimens made of FA-based geopolymer have lower mechanical properties [75]. Previous research on FA and slag mixtures also found that strength increased with increasing slag content [76–79]. This is due to an increase in calcium content in the mix with an increase in slag concentration. Ismail and Bernal [80] observed that calcium-rich pastes typically form a C-S-H gel, which forms a dense structure and increases strength. Nevertheless, as Si increases and calcium decreases, the Sodium-Alumino-Silicate-Hydrate (N-A-S-H) gel forms, resulting in a loss of strength. The compressive strength increases with slag content after seven and 28 days of curing.

Furthermore, the presence of CaO in slag encourages the hydration process, so a 100% slag content mixture has more compressive strength [81].

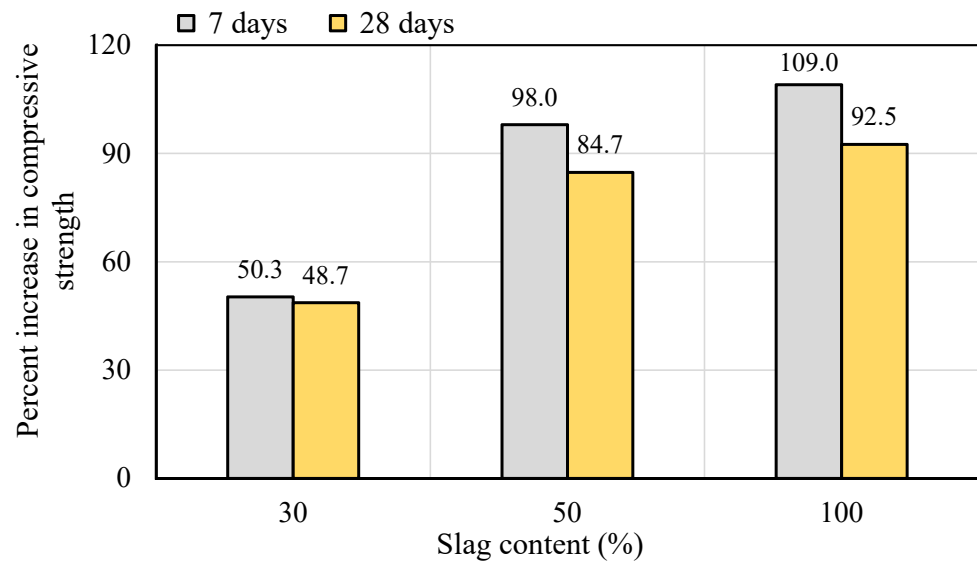


Figure 20. Percent increase in compressive strength vs. slag content.

5.2.2. Splitting Tensile Strength (f_t)

Figure 21 demonstrates the test values of splitting tensile strength (f_t), while Figure 22 shows the relative increase. It can be observed that increasing the slag content increases the splitting tensile. The maximum value of splitting achieved in this study was 5.60 MPa for the slag-based geopolymer concrete. The increase was 71.7%, 113.1%, and 123.1% for the G30, G50, and G100 mixes. It was also found that the increase in splitting values was 123% for the SCGC mixes having 100% slag content.

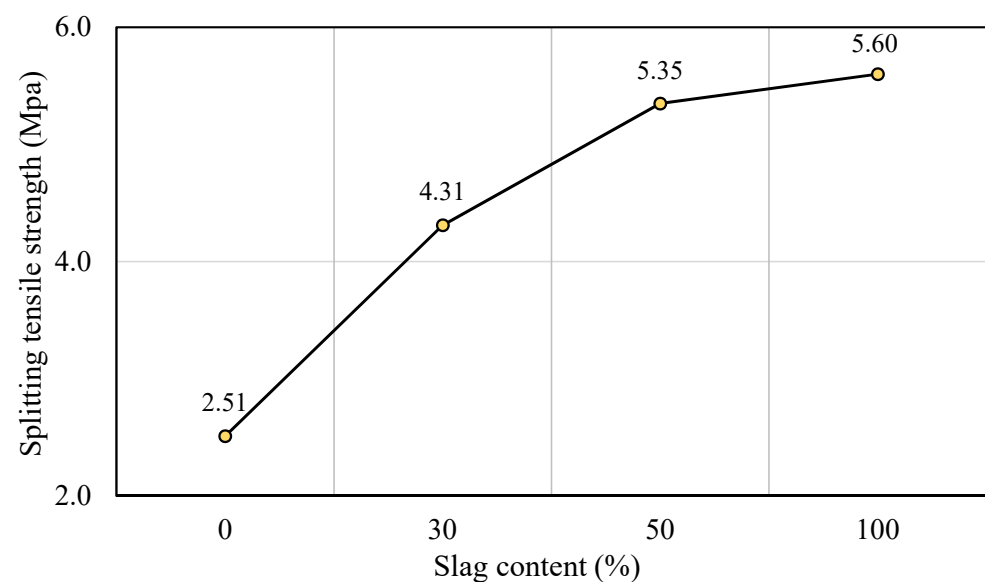


Figure 21. Influence of slag content on the compressive strength at 28 days.

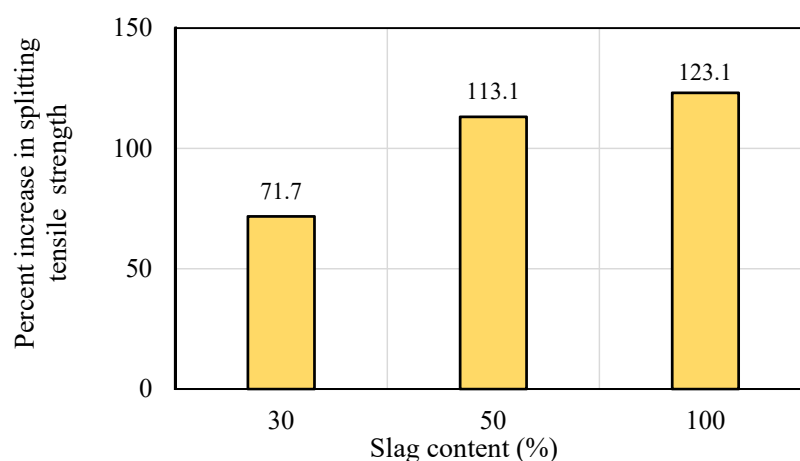


Figure 22. Percent increase in splitting tensile strength.

The 28-day failure surface of the SCGC specimens is shown in Figure 23. Coarse aggregate is equally distributed all across the specimens and does not segregate, except for the mix made with 100% FA, where a sign of segregation can be seen near the top casting side of the specimens. It is clear from Figure 23b,c, that for the mixes made with slag, the failure surface of SCGC specimens mostly went through the geopolymer paste matrix and the aggregates. However, in the FA-based geopolymer concrete mix (See Figure 23a), the failure path propagated through the interfacial transition zone and geopolymer paste matrix and rarely through the aggregates. This highlights the disparity in strength of geopolymer pastes of FA and slag-based mixes. According to Shen et al. [82], the surface's roughness and broken aggregates directly correlate with the splitting tensile strength. When the roughness is increased and more aggregates were cracked, the tensile splitting strength is higher [82]. The correlation between the splitting tensile and compressive strength in FA-based SCGC with various slag content is illustrated in Figure 24. It is obvious that an increase in compressive strength typically results in a corresponding subsequent increase in tensile strength [34]. Despite the usage of slag binder, the R-Square value of 0.994 indicates that the splitting and compressive strength values are strongly correlated with a direct linear relationship. For the results presented in Figure 24, the following correlation between splitting tensile strength and compressive strength was found:

$$f_t = 0.025f_{cu}^{1.225} \quad (8)$$

where f_t is the splitting tensile strength (MPa) and f_{cu} is the cube compressive strength (MPa).

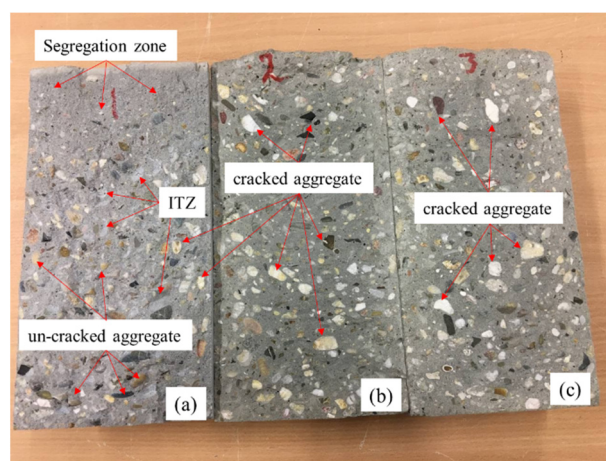


Figure 23. Failure path of splitting tensile strength test; (a) G0 (0% slag content), (b) G30 (30% slag content), and (c) G50 (50% slag content).

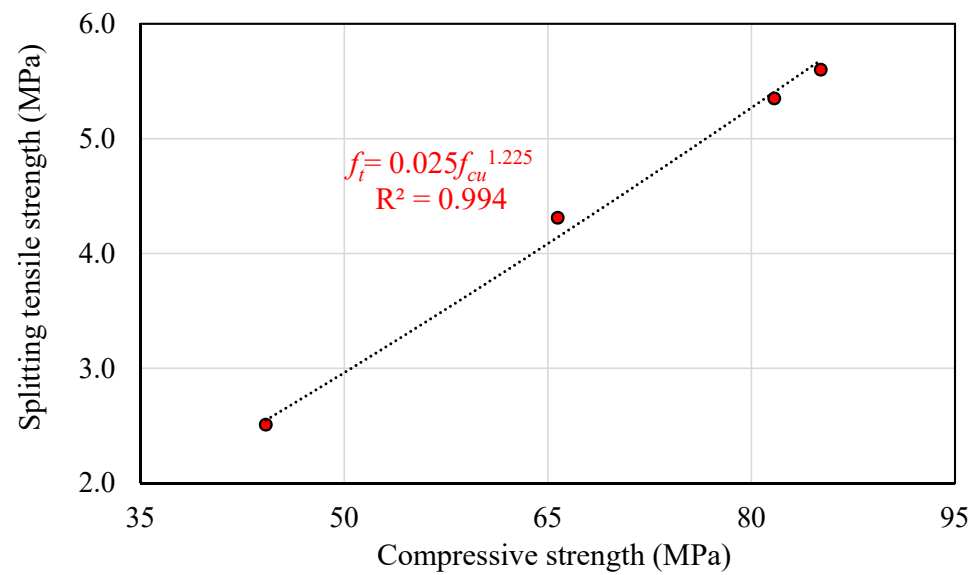


Figure 24. Correlation between splitting tensile and compressive strength.

5.3. Prediction of Splitting Tensile Strength

Though predictive equations for tensile strength exist for normal concrete, there is a lack of equations for geopolymer and self-compacted geopolymer concrete. The results from this study are compared with the results calculated from proposed equations by ACI 318-11 [61], ACI 363R-10 [62], Eurocode CEB-FIB [63], and Lee and Lee [64]. All the empirical models presented above were developed for normal concrete, except for the model proposed by Lee and Lee, which proposed for FA and slag blended geopolymer concrete. Figure 25 and Table 9 show the actual and predicted 28-day mechanical values using Equations (4)–(7) in Table 6 and a proposed model (Equation (8)).

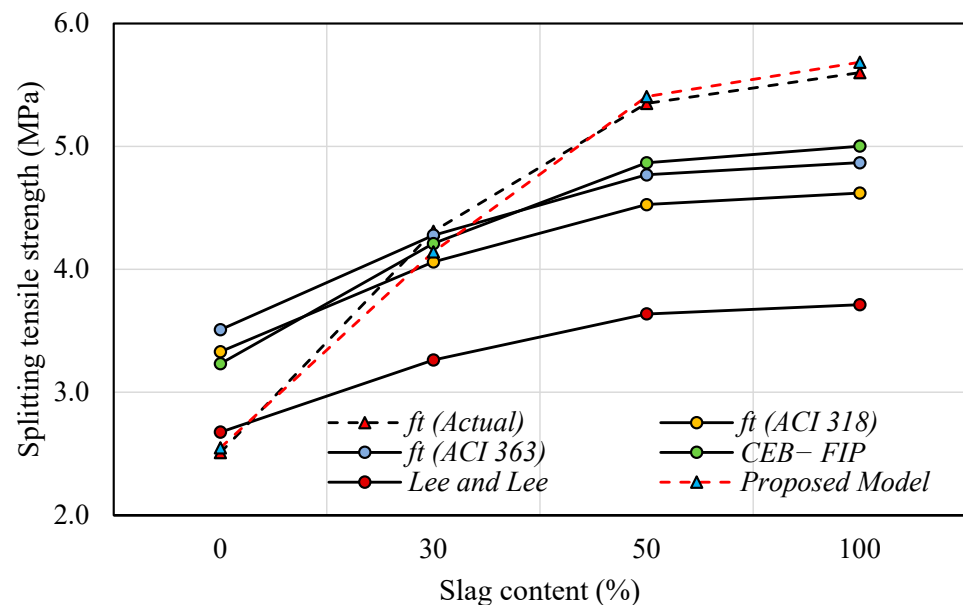


Figure 25. Actual and predicted splitting tensile strength values.

Table 9. Actual and predicted mechanical properties of SCGC recommended by ACI 318-11 [61], ACI 363R-10 [62], European code CEB-FIB [63], Lee and Lee [64], and self-developed model.

Mix Code	Slag Content (%)	Splitting Tensile Strength (MPa)					Proposed Model (Equation (8))
		Actual Result	ACI 318	ACI 363	CEB–FIP	Lee and Lee	
G0	0	2.51	3.33	3.51	3.23	2.68	2.55
G30	30	4.31	4.06	4.28	4.21	3.26	4.14
G50	50	5.35	4.53	4.77	4.87	3.64	5.41
G100	100	5.60	4.62	4.87	5.00	3.71	5.68

Splitting Tensile Strength (f_t)

Figure 25 compares the splitting tensile results obtained from this investigation versus predicted outcomes by ACI 318-11 [61], ACI 363R-10 [62], Eurocode CEB-FIB [63], Lee and Lee [64], and the proposed model (Equation (8)). For the reference mix G0, the tensile strength is close to the model that Lee and Lee proposed, while the predicted values by ACI models and CEB-FIB provide overestimates. However, surprisingly, the tensile strength predicted by Lee and Lee does not increase much with the compressive strength. The same can be said for the other predictions as well. This is because the splitting tensile strength in this study grows faster than the compressive strength. This is reflected in Equation 8 by the exponent of the compressive strength being higher than 1. This result is surprising, and indicates a more fundamental property of slag that enhances the tensile strength, possibly via the penetration of hydration products into the ITZ and aggregates themselves. This clearly requires further investigation.

The actual splitting tensile results of 70% FA and 30% slag mix are very similar to those predicted by ACI 318, ACI 363, and Eurocode CEB-FIB, but the proposed equations by Lee and Lee underestimate them. For instance, the experimental values were 5.8%, 0.7%, 2.3%, and 24.3% higher than the predicted values proposed by ACI 318, ACI 363, Eurocode CEB-FIB, and Lee and Lee, respectively, for the mix of 30% slag content. Using 50% and 100% slag content, the above variations between actual and predicted models become higher. However, ACI 363 and Eurocode CEB-FIB are the closest to the real values for G50 and G100 mixtures, which range between 9.0 and 13% lower than what was predicted. Faridmehr et al. [53] investigated SCGC made with the combined use of FA and slag. They also found that the proposed relationship by ACI 318 between compressive and splitting tensile strength does not correctly estimate the splitting tensile values of SCGC. Consequently, the above findings might help researchers predict the splitting tensile values of FA-based SCGC mixes made with or without slag with respect to the experimental compressive strength values, but to reach more decisive conclusions, more investigations and analysis are needed.

5.4. Durability Properties

Table 10 shows the capillary water absorption, free drying shrinkage, and mass loss results. The results indicate that increasing slag content reduces mass loss and capillary absorption but increases drying shrinkage.

Table 10. Results of durability properties of SCGC.

Mix Code	Slag Content (%)	Capillary Absorption(mm/min ^{0.5})	Free Drying Shrinkage after 365 Days	
			Max. Shrinkage (Microstrain)	Max. Mass Loss (g)
G0	0	0.0513	104	201
G30	30	0.0377	—	—
G50	50	0.0291	175	115
G100	100	0.0242	—	—

5.4.1. Capillary Water Absorption (Sorptivity)

Capillary water absorption tests determine SCGC's ability to absorb water from a single surface [83]. This index properly assesses the quality of the concrete surface layer, which controls reinforcement corrosion [83]. The lower the sorptivity, the more durable the concrete is and the better it performs in a harsh environment. The 28-day capillary water absorption coefficient for various slag contents is plotted in Figure 26. The relative decrease in capillary absorption coefficient is presented in Figure 27.

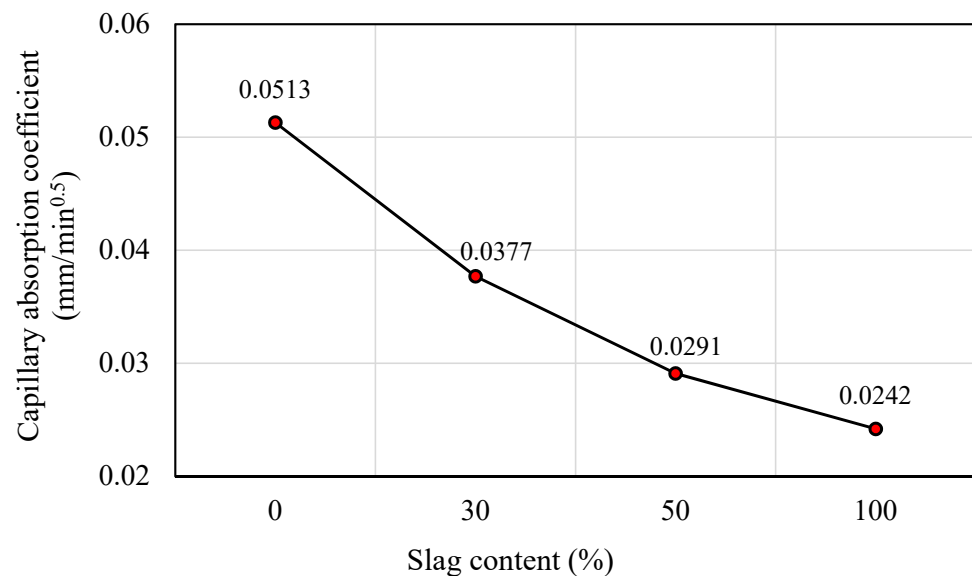


Figure 26. Influence of slag content on the capillary water absorption after 28 days.

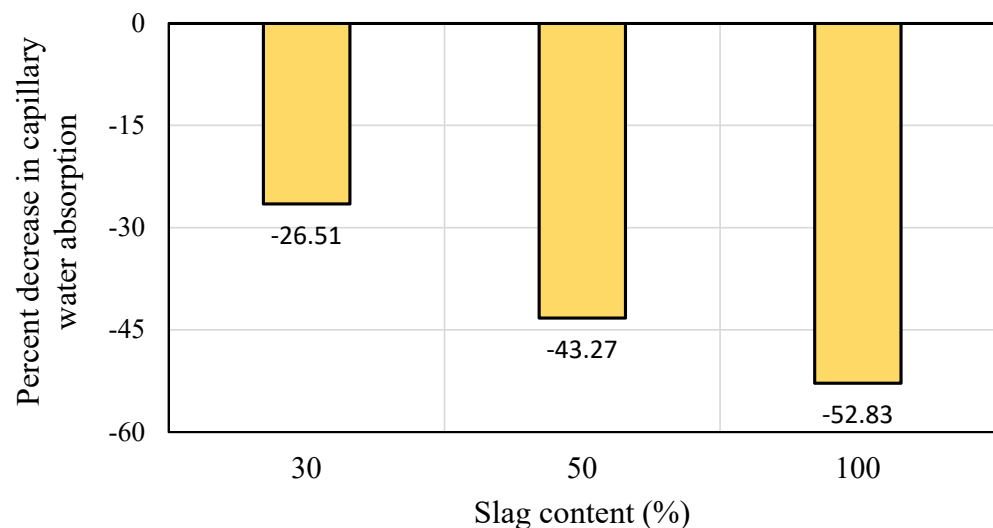


Figure 27. Percent decrease in capillary water absorption.

From the test results, a systematic decrease can be detected due to increased slag content. With the increasing of the slag content from 0 to 100%, a reduction in sorptivity of 52.83% is recorded. The trends observed in the results are in line with results by other researchers such as Shaikh [84], who found that geopolymer concrete displays lower sorptivity than normal concrete. Patel and Shah [4] studied blended FA and slag-based SCGC incorporating rice husk ash cured in ambient conditions. They reported that higher sorptivity is achieved by FA-based geopolymer concrete. The values of capillary suction for all SCGC specimens were in a range of 0.069–0.136 mm/min^{0.5}. According to recent research

on the effects of mineral admixtures on the characteristics of geopolymer concrete by Jindal et al. [85], raising the slag replacement ratio reduces the percentage of water absorption. Furthermore, permeability is determined by pore size distribution and structure. The pores' continuity influences water absorption. Geopolymer gel formation fills pores in the microstructure of the geopolymer concrete, changing the pore configuration and densifying the microstructure. As the age develops from 1 day to 28 days, the pores are gradually filled up by the production of geopolymer and C-S-H gels [4]. In geopolymer concrete, the slag binder provides the C-S-H gel formation, which holds CaO oxide in the chemical composition, resulting in enhanced strength.

5.4.2. Drying Shrinkage and Mass Loss

Curing is a key factor in evaluating the free drying shrinkage of concrete. It was previously reported that the shrinkage of geopolymers is highly dependent on the curing regime and liquid/binder ratio [86]. Additionally, the shrinkage of geopolymer mortar at a low temperature (40 °C) is very high compared to those cured at a higher temperature (60 °C) [86]. Furthermore, the compressive strength of geopolymer concrete improves with increasing curing temperature. The fib MC 2010 and B4 models both predict shrinkage based on the compressive strength [87]. For the above reasons, the effect of the curing condition and compressive strength on the shrinkage of geopolymer concrete is of great importance. Setting time and strength development of low-calcium FA-based geopolymer concrete is very low compared to blended FA and slag-based geopolymer concrete. Therefore, apart from the other parameters, different curing conditions were investigated in this study: (1) curing at an elevated temperature (85 °C), and (2) the prisms are cast for a free drying shrinkage test cured in an oven at a low temperature (40 °C) for three days. Figure 28 shows the compressive strength of 100 mm cubical specimens of the SCGC mixes cured at 40 °C for three days. The compressive strengths were enhanced by increasing slag content from 0% to 50%. A similar trend was reported in the previous sections of this paper.

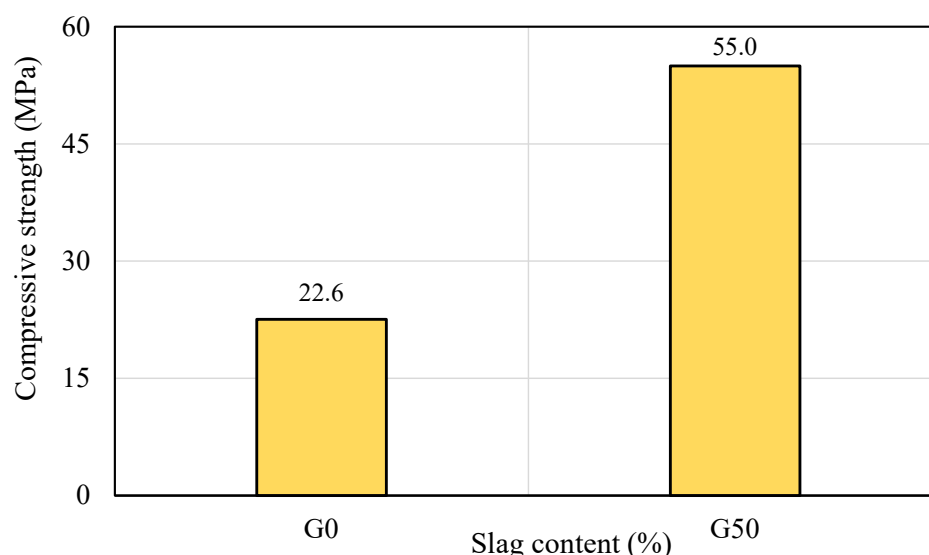


Figure 28. Compressive strength of SCGC specimens cured at 40 °C for three days.

Free Drying Shrinkage

Concrete drying shrinkage is characterized as a volumetric change as a result of concrete drying. Initially, free water is lost, resulting in minimal to no shrinkage. As the concrete continues to dry, the absorbed water is removed. Hydrostatic tension holds this adsorbed water in tiny capillaries. Tensile stresses are created when this water is lost, causing the concrete to shrink. The shrinkage caused by such a water loss is substantially more than the shrinkage caused by free water loss [88]. Drying shrinkage is a long-term process that depends on the water-cement ratio, hydration process, curing condition,

moisture content, drying interval, aggregate properties, additives, and chemical properties of the cement [89–91]. Typical curves of free drying shrinkage vs. drying time for the SCGC mixes with and without the inclusion of slag are given in Figure 29. Regardless of the slag content, a sharp increase in the free drying shrinkage test measurements is noticed up to 90 days of drying time; then, the curve becomes flat. The inclusion of slag in SCGC results in higher shrinkage values. The values of drying shrinkage at 365 days were 104 and 175 microstrain for the mix codes of G0 and G50, respectively. These values are lower than for OPC concrete. However, in a different study [70], it was reported that the drying shrinkage of FA-based geopolymer concrete cured in ambient conditions reduces with the addition of slag, and the six-month shrinkage of geopolymer concrete mixes ranged between 482 and 722 microstrain. Moreover, geopolymer concrete attained lower values of shrinkage compared to ordinary concrete for comparable compressive strength values. Additionally, it has been reported that the drying shrinkage strains of geopolymer concrete cured via oven are generally less than those concrete cured at ambient conditions [92]. Furthermore, it was reported that low-calcium binders are less reactive than high-calcium binders. In alkali-activated mixtures, class F fly ash reduced the shrinkage of concrete compared to class C fly ash and slag binders [93,94].

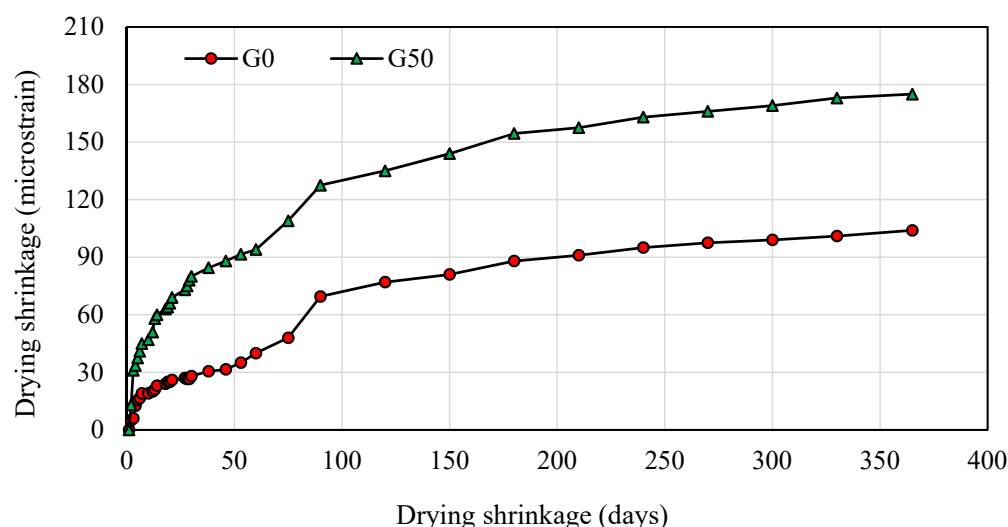


Figure 29. Drying shrinkage strain development of SCGC.

Mass Loss

The results of mass loss versus drying time are plotted in Figure 30. SCGC incorporating slag displayed a lower mass loss than the mix made with 100% FA. At 365 days, the mass losses of the mixes made of 0% and 50% slag were 201 g and 115 g, respectively. According to previous studies, there might not be a direct relationship between drying shrinkage and SCC's mass loss measurements. The mass loss indicator alone cannot provide substantial information on the variation in the drying shrinkage of concrete [95], as a number of other variables influence drying shrinkage in addition to mass loss [90,91]. The obtained behavior is contrary to expectations and there are no available studies regarding this property, hence more work is required in this direction.

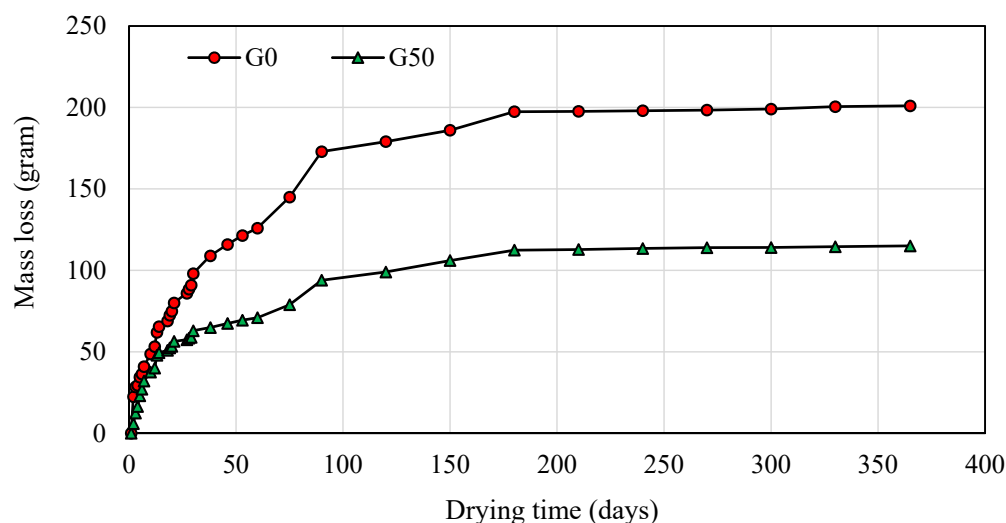


Figure 30. Mass loss variations of SCGC.

6. Conclusions

Based on the findings, the following conclusions can be drawn on the impact of slag content on the fresh and hardened qualities of SCGC containing FA:

1. Slag inclusion has a negative impact on the flowability of SCGC in terms of slump flow and J-ring flow diameter. The slump and J-ring flow values decrease by increasing the slag in the mixes, but this is still within EFNARC's acceptable limits. This may be due to the morphology, lower specific surface area, and lesser reactivity of the FA binder compared to slag.
2. T_{500} , TJ_{500} , and V-funnel flow times increase with the increase in slag replacement levels. The relationship of V-funnel via T_{500} and V-funnel via TJ_{500} also indicates that slag-rich SCGCs mixtures belong to the viscosity class (VS2/VF2) as defined by EFNARC. It can also be concluded that this kind of concrete might help improve resistance to segregation or reduce pressure on the formwork.
3. Slag leads to a reduction in the passing-ability of fresh concrete.
4. Slag has a significant impact on the segregation resistance of SCGC mixes. The allowable range of segregation index (%) is attained when the usage of slag exceeds 30% of the total binder content.
5. The low-calcium content of FA binders delays hardening, and using slag in geopolymer concrete mixes can help accelerate strength gain.
6. The utilization of slag results in a considerable increase in compressive and splitting tensile strength. The highest relative benefit is observed at 50% replacement.
7. The splitting tensile strength was found to increase faster than the compressive strength, indicating a potential enhancement of the ITZ. A new predictive equation is proposed for these mixes.
8. Based on the sorptivity test, a higher slag content enhances the durability of SCGC. By utilizing slag, SCGA specimens can achieve a higher rate of resistance to absorption. As the percentage of slag climbed from 0% to 100%, the sorptivity value declined to 48.5%.
9. FA-based SCGC made with or without slag exhibits low free drying shrinkage. SCGC made with 100% FA displays lower shrinkage strains than the mix made with 50% FA and 50% slag due to the lower reactivity of the FA binder compared to slag. After one year of exposing samples to drying conditions, the free drying shrinkage values of SCGC specimens cured at 40 °C were 104 and 175 microstrain for the G0 and G50 mixes, respectively.
10. Fully FA-based SCGC specimens show greater mass loss than the mix with 50% slag content. Therefore, it may be inferred that the mass loss parameter does not provide sufficient information about the variety in free drying shrinkage results.

7. Recommendations

It is recommended to investigate the influence of slag content on the durability performance of FA-based SCGC; specifically, gas permeability and rapid chloride permeability. In addition, further studies are needed on the long-term free drying shrinkage and mass loss. Furthermore, restrained shrinkage could be a topic of interest to the researchers. Investigating the microstructure of the FA-based SCGC with various slag content is also important to justify the behavior of the mechanical strength and durability of such mixes.

Author Contributions: Conceptualization, A.F.H.S., K.H.Y., R.W.A. and K.P.; methodology, A.F.H.S., K.H.Y., R.W.A. and K.P.; software, A.F.H.S., K.H.Y. and R.W.A.; validation, A.F.H.S., K.H.Y., R.W.A. and K.P.; formal analysis, A.F.H.S., K.H.Y. and R.W.A.; investigation, A.F.H.S., K.H.Y. and R.W.A.; resources, A.F.H.S., K.H.Y. and R.W.A.; data curation, A.F.H.S. and K.H.Y.; writing—original draft preparation, A.F.H.S., K.H.Y. and R.W.A.; writing—review and editing, A.F.H.S., K.H.Y., R.W.A. and K.P.; visualization, A.F.H.S., K.H.Y., R.W.A. and K.P.; supervision, K.H.Y., R.W.A. and K.P.; project administration, A.F.H.S., K.H.Y. and R.W.A.; funding acquisition, A.F.H.S., K.H.Y. and R.W.A. All authors have read and agreed to the published version of the manuscript.

Funding: This research received no external funding.

Institutional Review Board Statement: Not applicable.

Informed Consent Statement: Not applicable.

Acknowledgments: The authors would like to thank Soran University and Erbil Polytechnical University especially Bashdar A. Abdulla for supporting this research and the University of Applied Sciences Erfurt for their hospitality as well as administrative and practical support, especially Cornelia Witter from FHE International Office and Wolfgang Hezel from FHE Concrete laboratory.

Conflicts of Interest: The authors declare that they have no conflicts of interest.

Abbreviations

FA, Fly Ash; Slag, Ground Granulated Blast Furnace Slag; SCC, Self-Compacted Concrete; SCGC, Self-Compacted Geopolymer Concrete; ACI, American Concrete Institute; CEB-FIB, Constructions Électriques de Beaucourt-International Federation for Structural Concrete; OPC, Ordinary Portland Cement; Si, Silica; AL, Alumina; CaO, Calcium Oxide; CO₂, Carbon Dioxide; C-S-H, Calcium-Silicate-Hydrates; N-A-S-H, Sodium-Alumino-Silicate-Hydrate; NS, Nano-Silica; RHA, Rice Husk Ash; MK, Metakaolin; GSA, Groundnut Shell Ash; SF, Silica Fume; Na₂SiO₃, Sodium Silicate; NaOH, Sodium Hydroxide; Na₂O, Sodium Oxide; SiO₂, Silicon Dioxide; BS EN, British and European Standard Specifications; SP, Superplasticizer; EFNARC, European Federation of National Associations Representing for Concrete; PJ, J-ring Passing-ability; PA, L-box Passing-ability; SI, Sieve Segregation Index; f_{cu} , Cubical Compressive Strength; f_c , Cylindrical Compressive Strength; RH, Relative Humidity.

References

1. Antiohos, S.K.; Tapali, J.G.; Zervaki, M.; Sousa-Coutinho, J.; Tsimas, S.; Papadakis, V.G. Low Embodied Energy Cement Containing Untreated RHA: A Strength Development and Durability Study. *Constr. Build. Mater.* **2013**, *49*, 455–463. [\[CrossRef\]](#)
2. Prasittisopin, L.; Trejo, D. Hydration and Phase Formation of Blended Cementitious Systems Incorporating Chemically Transformed Rice Husk Ash. *Cem. Concr. Compos.* **2015**, *59*, 100–106. [\[CrossRef\]](#)
3. Aprianti, E.; Shafigh, P.; Bahri, S.; Farahani, J.N. Supplementary Cementitious Materials Origin from Agricultural Wastes—A Review. *Constr. Build. Mater.* **2015**, *74*, 176–187. [\[CrossRef\]](#)
4. Patel, Y.J.; Shah, N. Enhancement of the Properties of Ground Granulated Blast Furnace Slag Based Self Compacting Geopolymer Concrete by Incorporating Rice Husk Ash. *Constr. Build. Mater.* **2018**, *171*, 654–662. [\[CrossRef\]](#)
5. Rangan, B.V. *Fly Ash-Based Geopolymer Concrete*; Curtin University of Technology: Perth, Australia, 2010.
6. Davidovits, J. *Geopolymer Chemistry and Applications*, 3rd ed.; Geopolymer Institute: Saint-Quentin, France, 2011.
7. Ahmed, H.U.; Mahmood, L.J.; Muhammad, M.A.; Faraj, R.H.; Qaidi, S.M.; Sor, N.H.; Mohammed, A.S.; Mohammed, A.A. Geopolymer Concrete as a Cleaner Construction Material: An Overview on Materials and Structural Performances. *Clean. Mater.* **2022**, *5*, 100111. [\[CrossRef\]](#)
8. Ahmed, H.U.; Mohammed, A.S.; Faraj, R.H.; Qaidi, S.M.A.; Mohammed, A.A. Compressive Strength of Geopolymer Concrete Modified with Nano-Silica: Experimental and Modeling Investigations. *Case Stud. Constr. Mater.* **2022**, *16*, e01036. [\[CrossRef\]](#)

9. Ahmed, H.U.; Mohammed, A.S.; Qaidi, S.M.A.; Faraj, R.H.; Hamah Sor, N.; Mohammed, A.A. Compressive Strength of Geopolymer Concrete Composites: A Systematic Comprehensive Review, Analysis and Modeling. *Eur. J. Environ. Civ. Eng.* **2022**, *26*, 1–46. [\[CrossRef\]](#)
10. Ahmed, H.U.; Mohammed, A.A.S.; Rafiq, S.; Mohammed, A.A.S.; Mosavi, A.; Sor, N.H.; Qaidi, S.M.A.A. Compressive Strength of Sustainable Geopolymer Concrete Composites: A State-of-the-Art Review. *Sustainability* **2021**, *13*, 13502. [\[CrossRef\]](#)
11. Wongpa, J.; Kiattikomol, K.; Jaturapitakkul, C.; Chindaprasirt, P. Compressive Strength, Modulus of Elasticity, and Water Permeability of Inorganic Polymer Concrete. *Mater. Des.* **2010**, *31*, 4748–4754. [\[CrossRef\]](#)
12. Li, C.; Sun, H.; Li, L. A Review: The Comparison between Alkali-Activated Slag (Si + Ca) and Metakaolin (Si + Al) Cements. *Cem. Concr. Res.* **2010**, *40*, 1341–1349. [\[CrossRef\]](#)
13. Chindaprasirt, P.; De Silva, P.; Sagoe-Crentsil, K.; Hanjitsuwan, S. Effect of SiO₂ and Al₂O₃ on the Setting and Hardening of High Calcium Fly Ash-Based Geopolymer Systems. *J. Mater. Sci.* **2012**, *47*, 4876–4883. [\[CrossRef\]](#)
14. Mehta, A.; Williams, V.; Parajuli, B. Child with Dysuria and/or Hematuria. *Indian J. Pediatr.* **2017**, *84*, 792–798. [\[CrossRef\]](#) [\[PubMed\]](#)
15. Saha, S.; Rajasekaran, C. Enhancement of the Properties of Fly Ash Based Geopolymer Paste by Incorporating Ground Granulated Blast Furnace Slag. *Constr. Build. Mater.* **2017**, *146*, 615–620. [\[CrossRef\]](#)
16. Nath, P.; Sarker, P.K.; Rangan, V.B. Early Age Properties of Low-Calcium Fly Ash Geopolymer Concrete Suitable for Ambient Curing. *Procedia Eng.* **2015**, *125*, 601–607. [\[CrossRef\]](#)
17. Nath, P.; Sarker, P.K. Effect of GGBFS on Setting, Workability and Early Strength Properties of Fly Ash Geopolymer Concrete Cured in Ambient Condition. *Constr. Build. Mater.* **2014**, *66*, 163–171. [\[CrossRef\]](#)
18. Hadi, M.N.S.; Farhan, N.A.; Sheikh, M.N. Design of Geopolymer Concrete with GGBFS at Ambient Curing Condition Using Taguchi Method. *Constr. Build. Mater.* **2017**, *140*, 424–431. [\[CrossRef\]](#)
19. Sherwani, A.F.H.; Younis, K.H.; Arndt, R.W. Fresh, Mechanical, and Durability Behavior of Fly Ash-Based Self Compacted Geopolymer Concrete: Effect of Slag Content and Various Curing Conditions. *Polymers* **2022**, *14*, 3209. [\[CrossRef\]](#)
20. Okamura, H.; Ouchi, M. Self Compacting Concrete—Research Paper. *J. Adv. Concr. Technol.* **2003**, *1*, 5–15. [\[CrossRef\]](#)
21. Faraj, R.H.; Ali, H.F.H.; Sherwani, A.F.H.; Hassan, B.R.; Karim, H. Use of Recycled Plastic in Self-Compacting Concrete: A Comprehensive Review on Fresh and Mechanical Properties. *J. Build. Eng.* **2020**, *30*, 101283. [\[CrossRef\]](#)
22. Faraj, R.H.; Sherwani, A.F.H.; Daraei, A. Mechanical, Fracture and Durability Properties of Self-Compacting High Strength Concrete Containing Recycled Polypropylene Plastic Particles. *J. Build. Eng.* **2019**, *25*, 100808. [\[CrossRef\]](#)
23. Faraj, R.H.; Sherwani, A.F.H.; Jafer, L.H.; Ibrahim, D.F. Rheological Behavior and Fresh Properties of Self-Compacting High Strength Concrete Containing Recycled PP Particles with Fly Ash and Silica Fume Blended. *J. Build. Eng.* **2020**, *34*, 101667. [\[CrossRef\]](#)
24. Memon, F.A.; Nuruddin, F.; Shafiq, N.; Fareed Ahmed, M.; Nuruddin, M.F.; Shafiq, N. Compressive Strength and Workability Characteristics of Low-Calcium Fly Ash-Based Self-Compacting Geopolymer Concrete. *World Acad. Sci. Eng. Technol.* **2011**, *74*, 8–14.
25. Younis, K.H.; Salihi, K.; Mohammedameen, A.; Sherwani, A.F.H.; Alzebaree, R. Factors Affecting the Characteristics of Self-Compacting Geopolymer Concrete. *IOP Conf. Ser. Earth Environ. Sci.* **2021**, *856*, 012028. [\[CrossRef\]](#)
26. Astuti, P.; Afriansya, R.; Anisa, E.A.; Randisyah, J. Mechanical Properties of Self-Compacting Geopolymer Concrete Utilizing Fly Ash. *AIP Conf. Proc.* **2022**, *2453*, 020028. [\[CrossRef\]](#)
27. Nazari, A.; Torgal, F.; Cevik, A.; Sanjayan, J. Compressive Strength of Tungsten Mine Waste- and Metakaolin-Based Geopolymers. *Ceram. Int.* **2014**, *40*, 6053–6062. [\[CrossRef\]](#)
28. Gilbert, R.I. Creep and Shrinkage Models for High Strength Concrete—Proposals for Inclusion in AS3600. *Aust. J. Struct. Eng.* **2002**, *4*, 95–106. [\[CrossRef\]](#)
29. Srishaila, J.M.; Ahamed, P.U.; Vishwanath, K.N.; Prakash, P. Experimental Study on Workability and Strength Characteristics of Fly Ash and GGBS Based Self-Compacting Geo Polymer Concrete. *Int. J. Eng. Res. Dev.* **2014**, *10*, 68–77.
30. Wallah, S.E.; Rangan, B.V. *Low-Calcium Fly Ash-Based Geopolymer Concrete: Long-Term Properties*; Curtin University of Technology: Perth, Australia, 2006.
31. Olivia, M.; Nikraz, H. Properties of Fly Ash Geopolymer Concrete Designed by Taguchi Method. *Mater. Des.* **2012**, *36*, 191–198. [\[CrossRef\]](#)
32. Nuruddin, M.F.; Memon, F.A.; Shafiq, N.; Demie, S. Drying Shrinkage of Fly Ash-Based Self-Compacting Geopolymer Concrete. *Appl. Mech. Mater.* **2014**, *567*, 362–368. [\[CrossRef\]](#)
33. Wang, S.-D.; Pu, X.-C.; Scrivener, K.L.; Pratt, P.L. Alkali-Activated Slag Cement and Concrete: A Review of Properties and Problems. *Adv. Cem. Res.* **1995**, *7*, 93–102. [\[CrossRef\]](#)
34. Al-Rawi, S.; Tayşi, N. Performance of Self-Compacting Geopolymer Concrete with and without GGBFS and Steel Fiber. *Adv. Concr. Constr.* **2018**, *6*, 323–344. [\[CrossRef\]](#)
35. Gülşan, M.E.; Alzebaree, R.; Rasheed, A.A.; Niş, A.; Kurtoglu, A.E. Development of Fly Ash/Slag Based Self-Compacting Geopolymer Concrete Using Nano-Silica and Steel Fiber. *Constr. Build. Mater.* **2019**, *211*, 271–283. [\[CrossRef\]](#)
36. Nagaraj, V.K.; Babu, D.L.V. Assessing the Performance of Molarity and Alkaline Activator Ratio on Engineering Properties of Self-Compacting Alkaline Activated Concrete at Ambient Temperature. *J. Build. Eng.* **2018**, *20*, 137–155. [\[CrossRef\]](#)

37. Saini, G.; Vattipalli, U. Assessing Properties of Alkali Activated GGBS Based Self-Compacting Geopolymer Concrete Using Nano-Silica. *Case Stud. Constr. Mater.* **2020**, *12*, e00352. [\[CrossRef\]](#)
38. Ganeshan, M.; Venkataraman, S. Durability and Microstructural Studies on Fly Ash Blended Self-Compacting Geopolymer Concrete. *Eur. J. Environ. Civ. Eng.* **2019**, *25*, 2074–2088. [\[CrossRef\]](#)
39. Patel, Y.J.; Shah, N. Development of Self-Compacting Geopolymer Concrete as a Sustainable Construction Material. *Sustain. Environ. Res.* **2018**, *28*, 412–421. [\[CrossRef\]](#)
40. Manjunath, R.; Ranganath, R.V. Performance Evaluation of Fly-Ash Based Self-Compacting Geopolymer Concrete Mixes. *IOP Conf. Ser. Mater. Sci. Eng.* **2019**, *561*, 012006. [\[CrossRef\]](#)
41. Nuruddin, M.F.; Demie, S.; Shafiq, N. Effect of Mix Composition on Workability and Compressive Strength of Self-Compacting Geopolymer Concrete. *Can. J. Civ. Eng.* **2011**, *38*, 1196–1203. [\[CrossRef\]](#)
42. Demie, S.; Nuruddin, M.F.; Shafiq, N. Effects of Micro-Structure Characteristics of Interfacial Transition Zone on the Compressive Strength of Self-Compacting Geopolymer Concrete. *Constr. Build. Mater.* **2013**, *41*, 91–98. [\[CrossRef\]](#)
43. Reddy, K.M.; Kumar, G.N. Experimental Study on Self Compacting Geopolymer Concrete. *Int. J. Eng. Res.* **2017**, *4*, 953–957.
44. Bheel, N.; Awoyera, P.; Tafsirojjaman, T.; Hamah Sor, N.; sohu, S. Synergic Effect of Metakaolin and Groundnut Shell Ash on the Behavior of Fly Ash-Based Self-Compacting Geopolymer Concrete. *Constr. Build. Mater.* **2021**, *311*, 125327. [\[CrossRef\]](#)
45. Kamseu, E.; Ponzoni, C.; Tippayasam, C.; Taurino, R.; Chaysuwan, D.; Sglavo, V.M.; Thavorniti, P.; Leonelli, C. Self-Compacting Geopolymer Concretes: Effects of Addition of Aluminosilicate-Rich Fines. *J. Build. Eng.* **2016**, *5*, 211–221. [\[CrossRef\]](#)
46. Muttashar, H.L.; Ariffin, M.A.M.; Hussein, M.N.; Hussin, M.W.; Ishaq, S. Bin Self-Compacting Geopolymer Concrete with Spend Garnet as Sand Replacement. *J. Build. Eng.* **2018**, *15*, 85–94. [\[CrossRef\]](#)
47. Nurudin, M.F.; Memon, F.A.; Nuruddin, M.F.; Memon, F.A.; Nurudin, M.F.; Memon, F.A. Properties of Self-Compacting Geopolymer Concrete. *Mater. Sci. Forum* **2015**, *803*, 99–109. [\[CrossRef\]](#)
48. Sashidhar, C.; Guru Jawahar, J.; Neelima, C.; Pavan Kumar, D. Preliminary Studies on Self Compacting Geopolymer Concrete Using Manufactured Sand. *Asian J. Civ. Eng.* **2016**, *17*, 277–288.
49. Ushaa, T.G.; Anuradha, R.; Venkatasubramani, G.S. *Performance of Self-Compacting Geopolymer Concrete Containing Different Mineral Admixtures*; NISCAIR-CSIR: New Delhi, India, 2015; Volume 22.
50. Eren, N.A.; Alzebaree, R.; Çevik, A.; Niş, A.; Mohammedameen, A.; Gülşan, M.E. Fresh and Hardened State Performance of Self-Compacting Slag Based Alkali Activated Concrete Using Nanosilica and Steel Fiber. *J. Compos. Mater.* **2021**, *55*, 4125–4139. [\[CrossRef\]](#)
51. Memon, F.A.; Nuruddin, M.F.; Demie, S.; Shafiq, N. Effect of Superplasticizer and Extra Water on Workability and Compressive Strength of Self-Compacting Geopolymer Concrete. *Res. J. Appl. Sci. Eng. Technol.* **2012**, *4*, 407–414.
52. Arun, B.R.; Nagaraja, P.S.; Srishaila, J.M. *An Effect of NaOH Molarity on Fly Ash—Metakaolin-Based Self-Compacting Geopolymer Concrete*; Springer: Singapore, 2019; Volume 25, ISBN 9789811333170.
53. Faridmehr, I.; Nehdi, M.L.; Huseien, G.F.; Baghban, M.H.; Sam, A.R.M.; Algaifi, H.A. Experimental and Informational Modeling Study of Sustainable Self-Compacting Geopolymer Concrete. *Sustainability* **2021**, *13*, 7444. [\[CrossRef\]](#)
54. BS EN 933-1+A1 2005; Tests for Geometrical Properties of Aggregates—Part 1: Determination of Particle Size Distribution—Sieving Method. BSI Standards Publication: London, UK, 2008.
55. BS EN 1097-6; Tests for Mechanical and Physical Properties of Aggregates—Part 6: Determination of Particle Density and Water Absorption. BSI Standards Publication: London, UK, 2013.
56. Sata, V.; Wongs, A.; Chindaprasirt, P. Properties of Pervious Geopolymer Concrete Using Recycled Aggregates. *Constr. Build. Mater.* **2013**, *42*, 33–39. [\[CrossRef\]](#)
57. EFNARC. The European Guidelines for Self-Compacting Concrete. *Eur. Guidel. Self Compact. Concr.* **2005**, *22*, 63.
58. BS EN 12350-11; Testing Fresh Concrete—Part 11: Self-Compacting Concrete—Sieve Segregation Test. BSI Standards Publication: London, UK, 2010.
59. BS EN 12390-3; Testing Hardened Concrete—Part 3: Compressive Strength of Test Specimens. BSI Standards Publication: London, UK, 2009.
60. BS EN 12390-6:2000; Testing Hardened Concrete—Part 6: Tensile Splitting Strength of Test Specimens. BSI Standards Publication: London, UK, 1993.
61. ACI 318M-11; Building Code Requirements for Structural Concrete and Commentary. American Concrete Institute: Farmington Hills, MI, USA, 2011.
62. ACI 363 R-10; Report on High-Strength Concrete. American Concrete Institute: Farmington Hills, MI, USA, 2010.
63. Comité Euro-International du Béton. *CEB-FIP Model Code 1990: Design Code*; Thomas Telford Publishing: London, UK, 1993; ISBN 978-0-7277-3944-5.
64. Lee, N.K.; Lee, H.K. Setting and Mechanical Properties of Alkali-Activated Fly Ash/Slag Concrete Manufactured at Room Temperature. *Constr. Build. Mater.* **2013**, *47*, 1201–1209. [\[CrossRef\]](#)
65. İpek, S.; Ayodele, O.A.; Mermerdaş, K. Influence of Artificial Aggregate on Mechanical Properties, Fracture Parameters and Bond Strength of Concretes. *Constr. Build. Mater.* **2020**, *238*, 117756. [\[CrossRef\]](#)
66. BS EN 13057; Products and Systems for the Protection and Repair of Concrete Structures—Test Methods—Determination of Resistance of Capillary Absorption. BSI Standards Publication: London, UK, 2002.

67. Khatib, J.M.; Mangat, P.S. Absorption Characteristics of Concrete as a Function of Location Relative to Casting Position. *Cem. Concr. Res.* **1995**, *25*, 999–1010. [\[CrossRef\]](#)
68. Khatib, J.M.; Clay, R.M. Absorption Characteristics of Metakaolin Concrete. *Cem. Concr. Res.* **2004**, *34*, 19–29. [\[CrossRef\]](#)
69. ASTM:C157/C157M-08; Test Method for Length Change of Hardened Hydraulic-Cement Mortar and Concrete. ASTM International: West Conshohocken, PA, USA, 2008; Volume 8, pp. 1–7. [\[CrossRef\]](#)
70. Deb, P.S.; Nath, P.; Sarker, P.K. Drying Shrinkage of Slag Blended Fly Ash Geopolymer Concrete Cured at Room Temperature. *Procedia Eng.* **2015**, *125*, 594–600. [\[CrossRef\]](#)
71. BS EN 12350-8; Testing Self Compacting Concrete: Slump Flow Test. British Standards Institution: London, UK, 2010; pp. 5–8.
72. Mohammed, N.; Sarsam, K.; Hussien, M. The Influence of Recycled Concrete Aggregate on the Properties of Concrete. *MATEC Web Conf.* **2018**, *162*, 02020. [\[CrossRef\]](#)
73. BS EN 12350-9; Testing Fresh Concrete Self-Compacting Concrete. V-Funnel Test. British Standards Institution: London, UK, 2010.
74. Akgaoglu, T.; Qubukguoglu, B.; Awad, A. A Critical Review of Slag and Fly-Ash Based Geopolymer Concrete. *Comput. Concr.* **2019**, *24*, 453–458. [\[CrossRef\]](#)
75. Chi, M.; Huang, R. Binding Mechanism and Properties of Alkali-Activated Fly Ash/Slag Mortars. *Constr. Build. Mater.* **2013**, *40*, 291–298. [\[CrossRef\]](#)
76. Puertas, F.; Martínez-Ramírez, S.; Alonso, S.; Vázquez, T.; Martínez-Ramírez, S.; Alonso, S.; Vázquez, T.; Martínez-Ramírez, S.; Alonso, S.; Vázquez, T. Alkali-Activated Fly Ash/Slag Cements: Strength Behaviour and Hydration Products. *Cem. Concr. Res.* **2000**, *30*, 1625–1632. [\[CrossRef\]](#)
77. Qiu, J.; Zhao, Y.; Xing, J.; Sun, X. Fly Ash/Blast Furnace Slag-Based Geopolymer as a Potential Binder for Mine Backfilling: Effect of Binder Type and Activator Concentration. *Adv. Mater. Sci. Eng.* **2019**, *2019*, 2028109. [\[CrossRef\]](#)
78. Wang, W.C.; Wang, H.Y.; Lo, M.H. The Fresh and Engineering Properties of Alkali Activated Slag as a Function of Fly Ash Replacement and Alkali Concentration. *Constr. Build. Mater.* **2015**, *84*, 224–229. [\[CrossRef\]](#)
79. Sasui, S.; Kim, G.; Nam, J.; Koyama, T.; Chansomsak, S. Strength and Microstructure of Class-C Fly Ash and GGBS Blend Geopolymer Activated in NaOH & NaOH + Na₂SiO₃. *Materials* **2020**, *13*, 59. [\[CrossRef\]](#)
80. Ismail, I.; Bernal, S.A.; Provis, J.L.; San Nicolas, R.; Hamdan, S.; Van Deventer, J.S.J. Modification of Phase Evolution in Alkali-Activated Blast Furnace Slag by the Incorporation of Fly Ash. *Cem. Concr. Compos.* **2014**, *45*, 125–135. [\[CrossRef\]](#)
81. Samantasinghar, S.; Singh, S.P. Effect of Synthesis Parameters on Compressive Strength of Fly Ash-Slag Blended Geopolymer. *Constr. Build. Mater.* **2018**, *170*, 225–234. [\[CrossRef\]](#)
82. Shen, Q.; Chen, W.; Liu, C.; Zou, W.; Pan, L. The Tensile Strength and Damage Characteristic of Two Types of Concrete and Their Interface. *Materials* **2020**, *13*, 16. [\[CrossRef\]](#)
83. Atewi, Y.R.; Hasan, M.F.; Güneyisi, E. Fracture and Permeability Properties of Glass Fiber Reinforced Self-Compacting Concrete with and without Nanosilica. *Constr. Build. Mater.* **2019**, *226*, 993–1005. [\[CrossRef\]](#)
84. Shaikh, F.U.A. Effects of Alkali Solutions on Corrosion Durability of Geopolymer Concrete. *Adv. Concr. Constr.* **2014**, *2*, 109–123. [\[CrossRef\]](#)
85. Jindal, B.B.; Jangra, P.; Garg, A. Effects of Ultra Fine Slag as Mineral Admixture on the Compressive Strength, Water Absorption and Permeability of Rice Husk Ash Based Geopolymer Concrete. *Mater. Today Proc.* **2020**, *32*, 871–877. [\[CrossRef\]](#)
86. Ridditirud, C.; Chindaprasirt, P.; Pimraksa, K. Factors Affecting the Shrinkage of Fly Ash Geopolymers. *Int. J. Miner. Metall. Mater.* **2011**, *18*, 100–104. [\[CrossRef\]](#)
87. Caron, R.; Patel, R.A.; Dehn, F. Extension of the Fib MC 2010 for Basic and Drying Shrinkage of Alkali-Activated Slag Concretes. *Struct. Concr.* **2022**, *1*–14. [\[CrossRef\]](#)
88. Neville, A.M. *Concrete: Neville's Insights and Issues*; Thomas Telford Ltd.: London, England, 2006; ISBN 0727734687.
89. Shh, S.P.; Krguller, M.E.; Sarigaphuti, M. Effects of Shrinkage-Reducing Admixtures on Restrained Shrinkage Cracking of Concrete. *ACI Mater. J.* **1992**, *89*, 289–295. [\[CrossRef\]](#)
90. Wiegink, K.; Surendra, P.; Shah, S.M. Shrinkage Cracking of High-Strength Concrete. *ACI Mater. J.* **1996**, *93*, 409–415. [\[CrossRef\]](#)
91. Gesoğlu, M.; Özturan, T.; Güneyisi, E.; Gesoğlu, M.; Özturan, T.; Güneyisi, E.; Gesoğlu, M.; Özturan, T.; Güneyisi, E. Shrinkage Cracking of Lightweight Concrete Made with Cold-Bonded Fly Ash Aggregates. *Cem. Concr. Res.* **2004**, *34*, 1121–1130. [\[CrossRef\]](#)
92. Brito, M.E.; Case, E.; Kriven, W.M.; Salem, J.; Zhu, D. (Eds.) Developments in Porous, Biological and Geopolymer Ceramics. In Proceedings of the 31st International Conference on Advanced Ceramics and Composites, Daytona Beach, FL, USA, 21–26 January 2007; Volume 28.
93. Hossain, D.S.; Strength, K.M.A. Shrinkage and Early Age Characteristics of One-Part Alkali-Activated Binders with High-Calcium Industrial Wastes, Solid Reagents and Fibers. *J. Compos. Sci.* **2021**, *5*, 315.
94. Adesina, A.; Das, S. Drying Shrinkage and Permeability Properties of Fibre Reinforced Alkali-Activated Composites. *Constr. Build. Mater.* **2020**, *251*, 119076. [\[CrossRef\]](#)
95. Öz, H.Ö.; Gesoğlu, M.; Güneyisi, E.; Sor, N.H. Self-Consolidating Concretes Made with Cold-Bonded Fly Ash Lightweight Aggregates. *ACI Mater. J.* **2017**, *114*, 385–395. [\[CrossRef\]](#)